DOI: 10.1002/chem.200801868

Luminescent Bimetallic Lanthanide Bioprobes for Cellular Imaging with Excitation in the Visible-Light Range

Emmanuel Deiters, Bo Song, Anne-Sophie Chauvin, Caroline D. B. Vandevyver, Frédéric Gumy, and Jean-Claude G. Bünzli*[a]

Abstract: A series of homoditopic ligands H_2L^{CX} ($X=4$–6) has been designed to self-assemble with lanthanide ions (Ln^{III}), resulting in neutral bimetallic helicates of overall composition $[Ln_2(L^{CX})_3]$ with the aim of testing the influence of substituents on the photophysical properties, particularly the excitation wavelength. The complex species are thermodynamically stable in water ($\log\beta_{23}$ in the range 26–28 at pH 7.4) and display a metal-ion environment with pseudo-D_3 symmetry and devoid of coordinated water molecules. The emission of Eu^{III}, Tb^{III}, and Yb^{III} is sensitised to various extents, depending on the properties of the ligand donor levels. The best helicate is $[Eu_2(L^{C5})_3]$ with excitation maxima at 350 and 365 nm and a quantum yield of 9%. The viability of cervix cancer HeLa cells is unaffected when incubated with up to 500 μm of the chelate during 24 h. The helicate permeates into the cells by endocytosis and locates into lysosomes, which co-localise with the endoplasmatic reticulum, as demonstrated by counterstaining experiments. The relatively long excitation wavelength allows easy recording of bright luminescent images on a confocal microscope ($\lambda_{exc}=405$ nm). The new lanthanide bioprobe remains undissociated in the cell medium, and is amenable to facile derivatisation. Examination of data for seven Eu^{III} and Tb^{III} bimetallic helicates point to shortcomings in the phenomenological rules of thumb between the energy gap $\Delta E(^3\pi\pi^*-^5D_J)$ and the sensitisation efficiency of the ligands.

Keywords: cell imaging · confocal microscopy · helical structures · lanthanides · luminescence · time-resolved microscopy

Introduction

Lanthanide luminescent bioprobes (LLBs) are emerging as viable alternatives to existing organic dyes, because they are not very sensitive to photobleaching, which is particularly frustrating in time-lapse microscopy for instance, and possess long-lived excited states, in addition to displaying large Stokes' shifts upon ligand excitation.[1,2] The first property arises from the propensity of Ln^{III} excited states to efficiently deactivate long-lived ligand triplet states, which are preferred intermediates in photoinduced electronic rearrangements and subsequent covalent modification of the organic luminophore. The second feature allows time-resolved detection of the metal-centred luminescence leading to extremely low background and increased sensitivity, particularly when it is combined with spectral discrimination made possible thanks to the third advantage. The use of LLBs is well established for time-resolved luminescence immunoassays for more than 20 years.[3–5] Extensions to the detection of DNA hybridisation,[5–8] of enzyme activities[9] or of various intracellular analytes[9,10] are also well documented. These applications sometime take advantage of luminescence resonant energy transfer (LRET, or FRET—Förster resonant energy transfer) experiments[5,11] for which a combination of quantum dots and LLB appears to be particularly promising.[12] Moreover, new developments in circularly polarised luminescence may soon add another facet to these analyses, taking advantage of the inherent chirality of many biomolecules.[13] On the other hand, and despite some early attempts,[14–16] cell or organ imaging with luminescent LLBs did not generated much attention until the late 1990s.[17] A surge of interest in this matter has been recently triggered by Parker's work on cyclen derivatives (cyclen = 1,4,7,10-tetraazacyclododecane).[18,19] It is worth noting that despite the existence of the technology for more than 20 years, time--

[a] Dr. E. Deiters, Dr. B. Song, Dr. A.-S. Chauvin, Dr. C. D. B. Vandevyver, F. Gumy, Prof. Dr. J.-C. G. Bünzli
Laboratory of Lanthanide Supramolecular Chemistry
École Polytechnique Fédérale de Lausanne (EPFL)
LCSL-BCH 1401 (Switzerland)
Fax: (+41) 21-693-9825
E-mail: jean-claude.bunzli@epfl.ch

Supporting information for this article is available on the WWW under http://dx.doi.org/10.1002/chem.200801868.

resolved (or time-gated) microscopy[20] has not been systematically used in these investigations until very recently, despite its evident advantage when LLBs are involved.

The design of a LLB must obey several stringent requirements,[2] the chemical (i.e., coordinative) aspects of which are well mastered.[21] Several classes of strongly coordinating ligands are at hand, for example, polyaminocarboxylates, β-diketonates, macrocycles derived from cyclen or from azacoronands and cryptands, most of them relying on the concept of induced fit[22] to produce the desired coordination environment, which ideally must be saturated and rigid in order to minimise non-radiative losses.

In our laboratory, we have investigated the feasibility of self-assembly[23] to produce stable mono- and bimetallic lanthanide-containing edifices displaying programmed functionalities.[24] In particular, hexadentate ditopic ligands, derived from a pyridine substituted in the 2-position by a strongly coordinating group, for example, a carboxylic acid, and in the 6-position by a derivatised benzimidazole moiety, have proved to be an entire class of novel and versatile building blocks (see Scheme 1). Both symmetrical[25] and unsymmetrical[26] ligands indeed self-assemble with two lanthanide

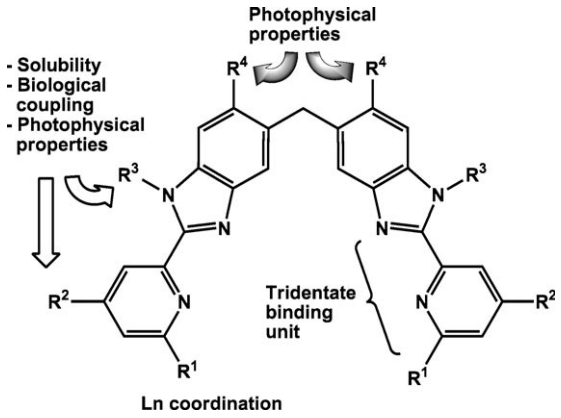

Scheme 1. General design of ditopic hexadentate receptors leading to the formation of bimetallic helicates $[Ln_2L_3]$.

ions, at room temperature, to yield homo- and heterobimetallic triple-stranded helicates, respectively, in which the nine-coordinate metal-ion environment has pseudo-tricapped trigonal prismatic geometry. This environment is especially protective so that remarkable luminescent properties follow suit. Another advantage of these bioprobes is the presence of two emissive centres, which could lead to bimodal probes, either dual luminescent or dual luminescent and magnetic; to our knowledge, such an approach for bioprobes has only been pursued by one other research group to date, which recently advocated the use of double lanthanide binding tags (dLBTs).[27]

The thermodynamic, photophysical, and biochemical properties of the homobimetallic helicates with the symmetrical receptors H_2L^{CX} ($X=1$, 2 or 3)[28] are adequate for cellular imaging. After self-assembly in water at pH 7.4, the helicates are the major species in solution, the quantum yields are large (10–24% for Eu^{III}), the luminescence of several other ions (e.g. Sm^{III}, Tb^{III}, Yb^{III}) is sensitised, lifetimes are long, for example, 2.2–2.4 ms for $Eu(^5D_0)$, and these entities permeate into the cytoplasm of several lines of cancerous (HeLa, MCF-7, Jurkat) and non-cancerous (HaCat) cells by endocytosis, while being non-cytotoxic ($IC_{50}>500$ μM).[28–31] The polyoxyethylene chain-fitting ligands H_2L^{CX} ($X=2$, 3) in addition to enhancing the solubility of the bimetallic LLBs, allows easy terminal derivatisation for coupling to bio-molecules and, if needed, it can be lengthened ($H_2L^{C2'}$) without substantially affecting the thermodynamic and photophysical properties of the helicates.[32] Among the chelates tested for cellular imaging, those with H_2L^{C2} have the best properties so far and when monitored under time-resolved conditions, images can be obtained for an incubation concentration as low as 5 μM.[33] An analytical protocol based on $[Eu_2(L^{C2})_3]$ has also been proposed for the detection of various DNAs and PCR products.[34]

The only drawback of the new class of bimetallic LLBs is common to many lanthanide luminescent tags, in that the excitation wavelength is in the UV range, with an absorption maximum around 320–325 nm. Luminescence microscopy can be performed by using 360 nm excitation, but this does not take full advantage of the photophysical properties of the helicates. Therefore in this paper, we explore the possibility of derivatising H_2L^{C2} in the R^4 position to shift the excitation wavelength towards the visible range; ligands H_2L^{CX} ($X=4$–6, Scheme 2) were synthesised and the effects of the substituent on the energy of the ligand levels and the quantum yields of the corresponding helicates were investi-

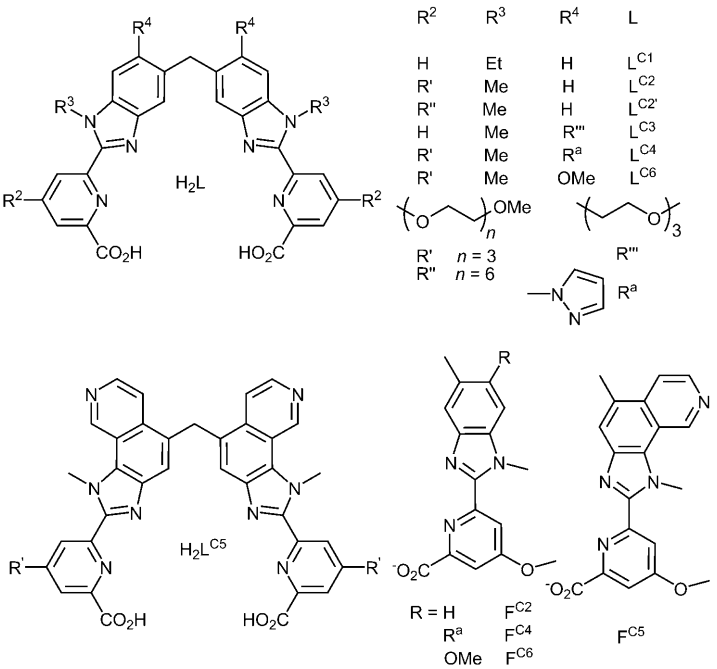

Scheme 2. Ditopic hexadentate ligands and fragments used for model calculations.

gated. Ligand H_2L^{C5} appears to be a good compromise between shifting the excitation into the visible (365 nm) and minimising the decrease in quantum yield. The cell permeation and imaging properties of $[Eu_2(L^{C5})_3]$ were therefore studied in detail, particularly with respect to its use in confocal microscopy.

Results

Ligand design and synthesis: Model calculations with CAChe® (at the PM3 level taking hydration into account) on representative fragments of the ligands (Scheme 2) allowed us to select H_2L^{CX} ($X=4$–6) as suitable candidates for the study. The syntheses of H_2L^{C4}–H_2L^{C6} generally adopted the same route as for ligand H_2L^{C2}.[29,31] The crucial idea consisted in introducing the poly(oxyethylene) substituents in the *para*-positions of the pyridine rings. The key intermediate **1** was obtained by selective hydrolysis and the carboxylic acid function was converted into acylchloride before condensation with the substituted bis(*N*-methylnitroaniline) intermediates I^{C4a}, I^{C5a} and I^{C6a} by means of a modified Phillips coupling reaction.[35] In the case of H_2L^{C6}, the synthetic route to **1** has been modified in order to improve the purity of its diethyl ester precursor, 4-{2-[2-(2-methoxyethoxy]ethoxy}pyridine-2,6-dicarboxylic acid diethyl ester: (triethyleneglycol)monomethyl ether tosylate was used and the tosyl group was substituted by the phenol group of the dipicolinic acid derivative in presence of caesium carbonate and DMF. The condensation products I^{C4b}, I^{C5b} and I^{C6c} were reduced in presence of iron to form the benzimidazole intermediates of I^{C4c}, I^{C5c} and I^{C6c}. The delicate operations during this step consist in 1) the removal of the product from the ferric aqueous phase and 2) preventing premature hydrolysis, otherwise an inseparable water soluble product forms. Final hydrolysis of the diester functions leads to the desired ligands with overall yields (steps i)–v) in Scheme 3) of 17, 7.5 and 49% for H_2L^{C4}, H_2L^{C5} and H_2L^{C6}, respectively.

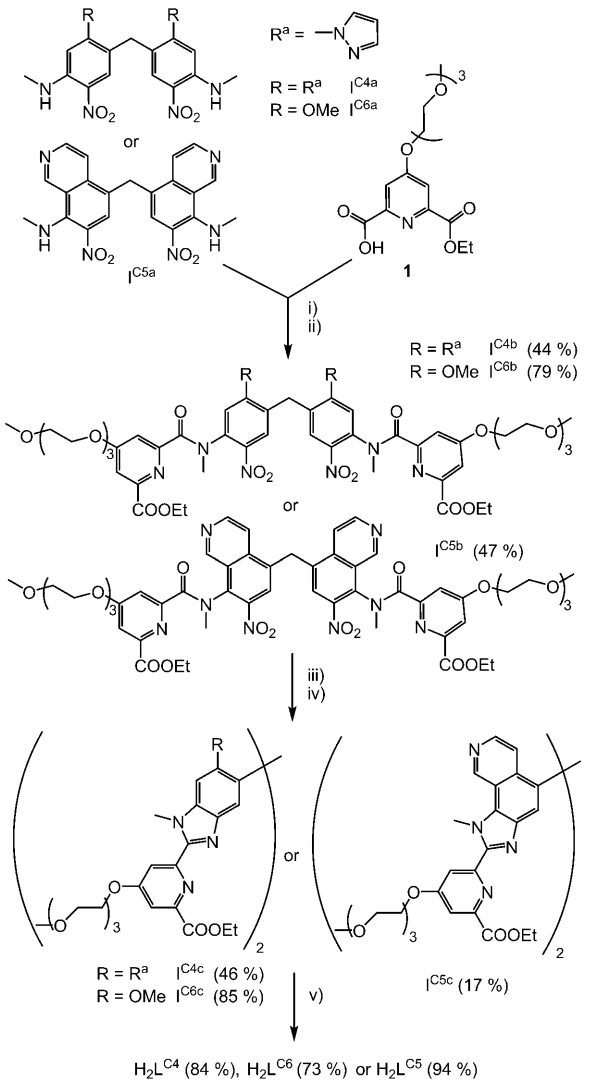

Scheme 3. Synthesis of the new ditopic ligands: i) $SOCl_2$ (10 equiv), DMF (0.1 equiv), **1** (2.6–2.7 equiv), CH_2Cl_2 (reflux, 2 h); ii) I^{C4a}, I^{C5a} or I^{C6a} (1 equiv), NEt_3/CH_2Cl_2, reflux (overnight); iii) Fe^0 (30 equiv), EtOH/H_2O/HCl, reflux (overnight); iv) EtOH/H_2SO_4 30:2 (v/v); v) NaOH (4.2 equiv, EtOH, RT, 2 h).

Helicate formation in water at pH 7.4: The self-assembly process between the ditopic ligands and lanthanide ions was studied by three different experimental techniques. Firstly, ^{1}H NMR spectra were recorded for 2:3 La/L stoichiometric solutions in D_2O. Contrary to the spectra of the ligands, which display broad and split bands reflecting conformational equilibria, as demonstrated by coalescence occurring at elevated temperatures, the data for the 2:3 Ln/L stoichiometric solutions display a main set of sharp signals. For instance, in the spectrum of the solution with H_2L^{C6} (Figure 1), the protons of the terminal methoxy groups of the polyoxyethylene pendants generate one sharp resonance, similarly to the protons of the NMe groups. In addition, the protons of the methylene bridge appear as a (slightly broadened) singlet at $\delta=3.38$ ppm. One may therefore conclude from this experiment that 1) the triple stranded $[La_2(L^{C6})_3]$ helicate is the major species in solution, 2) the three ligand strands are equivalent on the NMR timescale and 3) the overall symmetry of the molecular edifices is close to D_3. The small and weak resonances accompanying the main

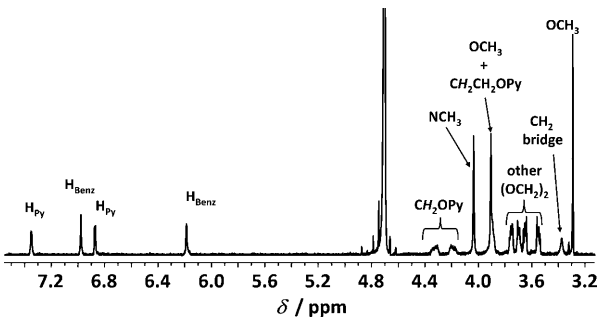

Figure 1. ^{1}H NMR spectrum of 2:3 stoichiometric solutions of $La(ClO_4)_3 \cdot nH_2O$ and H_2L^{C6} in D_2O at room temperature; $[La^{III}]_t = 6.9 \times 10^{-4}$ M.

peaks can be attributed to the minor species in solution (vide infra). Similar observations are made for the two other systems the spectra of which are displayed in Figure S1 in the Supporting Information. This conclusion is entirely supported by ESI-TOF mass-spectrometric data recorded on water/acetonitrile 90:10 (v/v) solutions with a total ligand concentration in the range $2.9–3.0\times10^{-4}$ M. For all investigated systems, a single Ln-containing species is seen, often as the base peak (Table 1, Tables S1–S3 in the Supporting Information), with the correct 2:3 stoichiometry. It is worth noting that no Ln-containing species with other stoichiometry appear in these spectra, at variance with, for instance, the solutions containing $H_2L^{C2'}$, for which both 2:3 and 2:2 species contributed to the ESI-MS spectra.[32] In the case of H_2L^{C5}, the helicate signal corresponds to the base peak for La and Eu, but not for Lu, for which apparently more dissociation occurs under the experimental conditions used, the base peak being assigned to the free ligand. A high resolution scan of two of the peaks attributed to $[Eu_2(L^{C5})_3]$ is shown on Figure 2 and the calculated isotopic distributions perfectly match the experimental ones.

Table 1. Major peaks corresponding to a Ln-containing species found in the ESI-TOF mass spectra of 2:3 Ln/L stoichiometric solutions in water/acetonitrile 90:10 with total ligand concentration $2.9–3.0\times10^{-4}$ M.

Species	m/z (obs.)	Intensity[a]	Assignment	m/z (calcd)	M_W [Da][b]
$[Eu_2(L^{C4})_3]$	1075.38	20	$[M+3H]^+/3$	1075.33	3222.97
	1089.68	45	$[M+2Na+H]^+/3$	1089.98	
$[La_2(L^{C5})_3]$	1036.66	100	$[M+3H]^+/3$	1036.59	3104.88
$[Eu_2(L^{C5})_3]$	1045.03	100	$[M+3H]^+/3$	1045.30	3132.91
$[Lu_2(L^{C5})_3]$	1060.38	60	$[M+3H]^+/3$	1060.64	3176.95
$[Eu_2(L^{C6})_3]$	1003.34	100	$[M+3H]^+/3$	1003.26	3006.90

[a] In percentage of base peak. [b] Molecular weight of the parent species.

To further confirm the predominance of the helicates in the investigated solutions, conditional stability constants were determined at pH 7.4 in Tris-HCl buffer by titrating H_2L^{CX} 1.21×10^{-5} M ($X=4$), 8.88×10^{-6} M ($X=5$) or 8.52×10^{-6} M ($X=6$) with concentrated solutions ($\approx5\times10^{-3}$ M) of lanthanide perchlorates (Ln = La, Eu, Lu) for ratios $R=[Ln]_t/[H_2L^{CX}]_t$ ranging between 0 and 4.

Factor analysis pointed to the presence of 4–6 absorbing species in solution and several models were tested for the least-squares fit of the data. Introduction of a 2:2 species, which has been identified previously[32] and which is an important reaction intermediate in the formation of the $[Eu_2(L^{C1})_3]$ helicate,[36] systematically led to non-convergence of the fitting procedure. Therefore the following model was retained [Eqs. (1)–(3); charges are omitted for clarity reasons].

$$2\,L^{CX} + Ln \rightleftharpoons [Ln(L^{CX})_2] \quad \log\beta_{12} \tag{1}$$

$$3\,L^{CX} + 2\,Ln \rightleftharpoons [Ln_2(L^{CX})_3] \quad \log\beta_{23} \tag{2}$$

$$L^{CX} + 2\,Ln \rightleftharpoons [Ln_2(L^{CX})] \quad \log\beta_{21} \tag{3}$$

The corresponding overall stability constants are reported in Table 2, while typical examples of the titrations are presented in Figures S2–S4 in the Supporting Information, along with distribution diagrams. The distribution diagram for the Eu^{III}/H_2L^{C5} system is reproduced on Figure 3. Interpretation of the stability constants must be done with care, in that the recalculated spectra of the various species are heavily correlated (Figure S5 in the Supporting Information). The general trend that emerges from the data of Table 2 is that substitution does not influence much the speciation with respect to $[Ln_2(L^{C2})_3]$. The stability of the 2:3 species appears to be larger by 2–3 orders of magnitude, when compared to the helicate with H_2L^{C2}; on the other hand, the stability of the 1:3 species is 3–4 orders of magnitude lower. However, $\log\beta_{21}$ is larger by 2–3 units, so that when the speciation is calculated for a total ligand concentration of 4.5×10^{-4} M, the proportion of bimetallic helicate in solution tends to be somewhat smaller than in the case of H_2L^{C2}, especially for H_2L^{C6}. Regarding the more interesting

Table 2. Conditional stability constants determined by spectrophotometric titrations in Tris-HCl 0.1 M (pH 7.4) at room temperature with standard deviations between parentheses, and percentages of the Eu-containing species.

Ligand		La	Eu	Lu	Eu species [%][a]
H_2L^{C2b}	$\log\beta_{13}$	18.8(2)	18.1(2)	18.7(3)	2.1
	$\log\beta_{23}$	24.9(4)	25.5(4)	26.3(4)	97.1
	$\log\beta_{21}$	11.7(3)	11.8(5)	12.4(2)	0.5
H_2L^{C4}	$\log\beta_{12}$	14.2(3)	14.8(4)	13.6(1)	5.9
	$\log\beta_{23}$	28.1(4)	28.5(5)	26.3(2)	92.5
	$\log\beta_{21}$	13.6(3)	14.3(3)	14.3(1)	0.9
H_2L^{C5}	$\log\beta_{12}$	14.0(1)	14.3(3)	n.a.	4.5
	$\log\beta_{23}$	27.4(3)	28.6(5)	28.8(3)	94.6
	$\log\beta_{21}$	15.9(1)	14.4(5)	16.0(3)	0.8
H_2L^{C6}	$\log\beta_{12}$	n.a.	14.0(1)	n.a.	9.1
	$\log\beta_{23}$	n.a.	27.9(1)	n.a.	88.7
	$\log\beta_{21}$	n.a.	15.4(1)	n.a.	1.5

[a] For $[H_2L^{CX}]_{tot}=4.5\times10^{-4}$ M. [b] From reference [31].

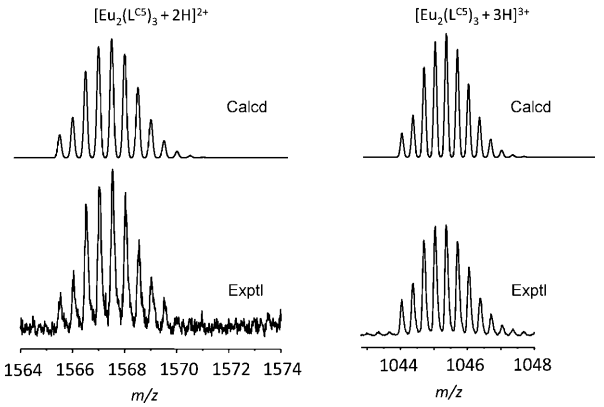

Figure 2. Experimental and calculated isotopic distribution for two signals assigned to the $[Eu_2(L^{C5})_3]$ species.

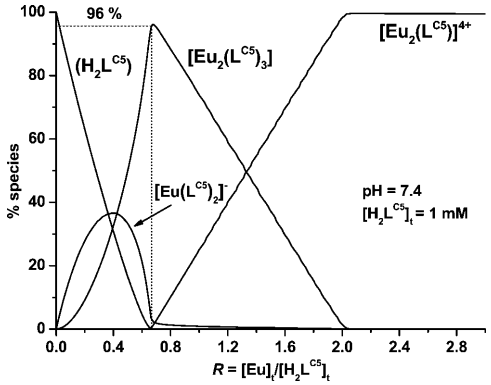

Figure 3. Distribution diagram of the Eu^{III}/H_2L^{C5} system computed with the conditional stability constants reported in Table 2 and for a total ligand concentration of 1 mM.

H_2L^{C5} ligand (vide infra), this species accounts for ≈95% of the speciation, a value compatible with in vitro experiments with live cells, for which incubation concentrations of the lanthanide bioprobes are usually in the range 50–200 μM.[28]

As for the previously reported bimetallic chelates bearing polyoxyethylene side arms,[30–32] no single crystals suitable for X-ray analysis could be grown, most probably in view of the presence of the six fluxional pendants. To ascertain the composition of the inner coordination sphere of the Eu^{III} helicates, high-resolution luminescence spectra have therefore been recorded at 10 K on frozen solutions in water/glycerol (9:1, v/v). They were analysed in terms of group-theory considerations[37] and compared to the spectrum of $[Eu_2(L^{C1})_3]$ for which lanthanide-induced shift analysis has demonstrated that the solution structure is very close to the available crystal structures.[25] For instance, the emission spectrum of the helicate with H_2L^{C5} (Figure 4) can be interpreted in terms of an emissive metal ion lying in a site with pseudo-D_3 symmetry. Firstly, the unique and symmetrical $^5D_0 \rightarrow {}^7F_0$ transition points to the presence of a single major species in solution. At room temperature, the energy of this transition is 17242 cm^{-1}, a value which is reasonably close to

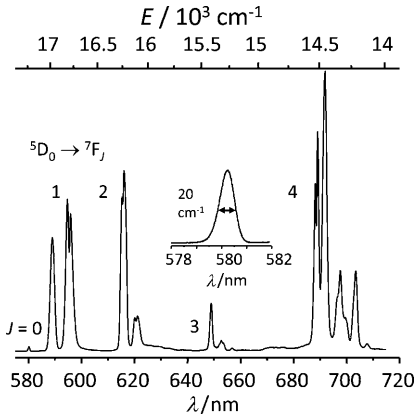

Figure 4. High-resolution emission spectrum of $[Eu_2(L^{C5})_3]$ 2.67×10^{-4} M in water/glycerol 9:1 (v/v) at 10 K under ligand excitation at 350 nm. The inset shows the $^5D_0 \rightarrow {}^7F_0$ transition.

the estimate made with a phenomenological equation[38] based on the nephelauxetic effect generated by six aromatic nitrogen ($\delta_{bzp} = -15.3\ cm^{-1}$) and three carboxylate oxygen ($\delta_{carb} = -17.2\ cm^{-1}$) donor atoms: 17231 cm^{-1}. Secondly, the $^5D_0 \rightarrow {}^7F_1$ transition is split into two main transitions, corresponding to ligand-field sublevels for $^7F_1$ located at 260 (irreducible representation A in D_3) and 437 cm^{-1} (E), respectively. The energy difference $\Delta E(A-E) = 177\ cm^{-1}$ is proportional to the ligand-field strength. An additional splitting is seen for $^7F_1$(E), the magnitude of which is a good indication of the extent of distortion with respect to the idealised symmetry: its actual value, 34 cm^{-1}, is close to the one observed for $[Eu_2(L^{C1})_3]$ (28 cm^{-1}, Table 3). Thirdly, the splitting observed for the other transitions ($J = 2$–4) is also compatible with the group-theory predictions for a pseudo-D_3 symmetry. A similar analysis conducted for the two other helicates ($X = 4$, 6; Figure S6 in the Supporting Information, Table 3) meets the same conclusions. Finally, all the luminescence decays measured at 10 K are single exponential functions and the lifetimes are long, 2.7–3.0 ms, reflecting an efficient protection of the metal ion from both inner- and outer-sphere interaction with water molecules (Table 3). Therefore the spectroscopic data gathered (NMR, UV/Vis, ESI-MS, luminescence) are all consistent with the formation of $[Ln_2(L^{CX})_3]$ helicates by self-assembly in aqueous solution, at physiological pH, as well as with the presence of two indistinguishable metal ion sites for the metal ions. Minor species may be present, but their concentration is small so that they remain undetected by most of the experimental techniques.

Table 3. Parameters for the symmetry analysis of the metal ion centres in $[Ln_2(L^{CX})_3]$ ($X = 4$–6) 2.67–2.76×10^{-4} M in water/glycerol 9:1 (v/v) at 10 K.

Helicate	$^5D_0 \rightarrow {}^7F_0$ E_{exptl} [cm^{-1}][a]	$^5D_0 \rightarrow {}^7F_0$ fwhh [cm^{-1}]	$^5D_0 \rightarrow {}^7F_1$ ΔE(A–E) [cm^{-1}]	$^5D_0 \rightarrow {}^7F_1$ ΔE(E–E) [cm^{-1}]	$\tau(^5D_0)$ [ms]
$[Eu_2(L^{C1})_3]$[b]	17 232	15	171	28	2.69±0.01
$[Eu_2(L^{C4})_3]$	17 242	20	181	26	2.9±0.1
$[Eu_2(L^{C5})_3]$	17 242	20	177	34	2.75±0.10
$[Eu_2(L^{C6})_3]$	17 237	17	160	31	2.8±0.1

[a] At 295 K, theoretical value: 17 231 cm^{-1}. [b] In Tris-HCl 0.1 M; all data at 295 K.

Photophysical properties: Before embarking on the labor-extensive covalent synthesis of the ditopic ligands, predictive calculations were performed with the CAChe® 7.5 package on the core fragments F^{CX} ($X = 2$, 4–6, Scheme 2) that are responsible for their photophysical properties. Ground-state geometries in water were optimised with the PM3/CI procedure and absorption spectra calculated with MOSF/CI at PM3 geometry. Our interest being in an excitation of the helicate as far as possible in the visible region, we focus on the maximum of the absorption band with the smallest energy. The corresponding calculated wavelengths match the experimental ones fairly well for fragments F^{C2}, F^{C5} and

F^{C6}: 311.5, 351 and 320.5 nm, respectively, compared to 307, 351.5 and 322.5 nm, respectively; that is, $\Delta\lambda$ is in the range 0.5–4.5 nm only. However, the predicted value for F^{C4} (347 nm) is much bigger than the measured one (319.5 nm); this large discrepancy may arise from the pyrazolyl fragment adopting, in aqueous solution, a conformation such that the electronic communication with the remaining part of the molecule is interrupted and which is not well reproduced by the calculations.

The uncomplexed ditopic ligands display three main absorption domains, 200–225, 230–280, and 300–370 nm, approximately, displaying one or more maxima. They are listed in Table 4, along with the energy of the singlet and triplet states. The bands at lower energy arise from $\pi\rightarrow\pi^*$ transitions involving intramolecular electron transfer from the benzimidazole moiety to the pyridine and carboxylate groups. Complexation to lanthanide ions results in a bathochromic shift of about 1100–1350 cm^{-1} for H_2L^{C4} and 1450–1600 cm^{-1} for H_2L^{C6}, depending on the lanthanide ion. In the case of H_2L^{C5}, the band at lower energy displays two maxima separated by 1000 cm^{-1}, which are little affected by complexation, the bathochromic shift being around 50–150 cm^{-1} for the high energy component and 250–350 cm^{-1} for the other. We note that the molar absorption coefficients of the helicates are large and range between $\log\varepsilon = 4.89$ and 4.97, which is an interesting property for the overall efficiency of luminescent probes.

Table 4. Photophysical properties of the ligands and their La^{III} or Gd^{III} complexes in aqueous Tris-HCl 0.1 M at 298 K.

Species	$E(^*\pi\leftarrow\pi)$[a] [cm^{-1}]	$\log\varepsilon$	$E(^1\pi\pi^*)$ [cm^{-1}][b]	$E(^3\pi\pi^*)$ [cm^{-1}][c]	$\tau(^3\pi\pi^*)$ [ms][d]	ΔE [cm^{-1}][e]
H_2L^{C4}	32 550	4.65	24 850, 25 950	20 400, 21 050	276(16)	4450
$[La_2(L^{C4})_3]$	31 450	4.97	23 700, n.a.	19 900, 21 150	272(23)	3800
H_2L^{C5}	28 550	4.36	25 150, 26 150	19 600, 20 800	350(50)	5550
	27 550	4.29			140(20)	
$[Gd_2(L^{C5})_3]$	28 500	4.90	24 750, n.a.	19 400, 20 800	75.9(5)	5350
	27 300	4.82				
H_2L^{C6}	30 950	3.52	22 100, n.a.	19 100, 20 300	990(80)	3000
$[Gd_2(L^{C6})_3]$	29 500	4.89	22 300, n.a.	18 650, 19 950	5.4(0.2)	4850

[a] Lowest energy transition. [b] From fluorescence spectra at 298 K; λ_{exc} = 307 (H_2L^{C4}), 350 (H_2L^{C5}), 323 (H_2L^{C6}) nm, and 319–321, 351–352, 339–341 nm for the corresponding helicates. [c] From phosphorescence spectra at 77 K, maximum of band envelope and 0-phonon transition, same λ_{exc} as for fluorescence spectra. [d] At 77 K. [e] $\Delta E = E(^1\pi\pi^*) - E(^3\pi\pi^*)$.

Upon excitation in the lower electronic states, all three ligands emit a broad, mainly featureless band (except for H_2L^{C5}) in the range 350–500 nm with maxima around 400 nm (H_2L^{C4}, H_2L^{C5}) or 450 nm (H_2L^{C6}). This band disappears upon enforcement of a time delay and is therefore assigned to emission from singlet state(s). At 77 K, time-gated luminescence spectra display a broad band with vibrational structure, which extends from 420–650 nm with maxima in the range 490–520 nm, and which arises from triplet state(s), since the corresponding lifetime is long (270–990 ms). The singlet state of the non-luminescent helicates (La^{III}, Gd^{III}, Lu^{III}) is somewhat red-shifted (1150 cm^{-1} for H_2L^{C4}, and 400 cm^{-1} for H_2L^{C5}), while the energy of the triplet state is almost unchanged ($\pm$400 cm^{-1}). Roughly speaking, the energy gap between the singlet and triplet states lies in the range 4000–5000 cm^{-1} in the helicates, a value favourable for efficient intersystem crossing, which often plays a major role in the overall ligand-to-metal energy-transfer process. The triplet state lifetime is also affected by the complexation, particularly in the case of Gd^{III} for which the lifetimes are quite short due to the heavy atom effect of the paramagnetic metal ion[39] (Table 4). In the case of the luminescent helicates, the emission from the ligand is almost completely quenched for Eu^{III}, with concomitant appearance of the sharp f–f transitions. This is not true for Tb^{III} for which ligand emission is seen with a large, small and very small intensity for H_2L^{C6}, H_2L^{C5} and H_2L^{C4}, respectively. For H_2L^{C5}, for instance, the decrease in singlet state emission amounts to 99.9 and 98% for $[Eu_2(L^{C5})_3]$ and $[Tb_2(L^{C5})_3]$, respectively. All three Yb^{III} helicates still display intense ligand emission, despite the observation of a relatively strong and well-defined $^2F_{5/2}\rightarrow{}^2F_{7/2}$ transition (Figure 5). It is also worth noting that the excitation spectra of the helicates with luminescent lanthanide ions perfectly match the absorption spectra, proving sensitisation of the luminescence by the ligands (Figures S7–S9 in the Supporting Information).

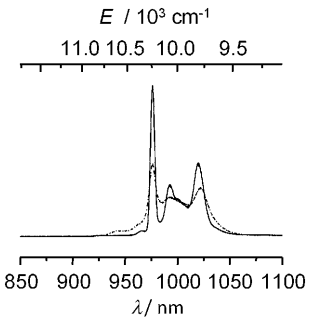

Figure 5. Emission of the Yb^{III} ion in a solution of $[Yb_2(L^{C5})_3]$ 2.8×10^{-5} M in Tris-HCl 0.1 M; excitation wavelength: 352 nm; solid line: 77 K, dotted line: 295 K.

The emission spectra of 10^{-4}–10^{-5} M solutions of the Eu^{III} helicates in Tris-HCL (0.1 M) at room temperature are very similar to those recorded on frozen solutions at 10 K, but for the expected broadening due to vibronic contributions[40] and to an increase in the $^5D_0\rightarrow{}^7F_2/{}^5D_0\rightarrow{}^7F_1$ intensity ratio, for the same reason. Similar conclusions can be drawn for the Tb^{III} helicates. To further prove the protective encapsulation of the Ln^{III} ions by the self-assembled nine-coordinate chemical environment, we recorded the luminescence

decays in water and in deuterated water, both at room temperature and 77 K. This allows us to determine the number of coordinated water molecules q and to assess the importance of other non-radiative deactivation processes, in particular phonon-assisted back transfer of the excitation energy onto the ligands. The relevant data are listed in Table 5 in which the reported q values have been calculated

Table 5. Lifetimes τ of the ^5D_J levels in water and deuterated water, hydration numbers q, and overall quantum yields for solutions of $[Ln_2(L^{CX})_3]$ helicates 10–15 μM in Tris-HCl (or DCl) 0.1 M, under ligand excitation, at 295 K.

Helicate	$\tau(H_2O)$ [ms]	$\tau(D_2O)$ [ms]	q (±0.3)[a]	Q^L_{Ln} [%]
$[Eu_2(L^{C4})_3]$	2.52 ± 0.02	4.34 ± 0.03	-0.1	15 ± 2
	2.68 ± 0.08	4.03 ± 0.09	(-0.2)[c]	15 ± 2
$[Tb_2(L^{C4})_3]$	0.12 ± 0.01	0.17 ± 0.01	[b]	2.5 ± 0.3
	2.58 ± 0.02[c]	2.67 ± 0.03[a]	(-0.2)[c]	
$[Eu_2(L^{C5})_3]$	2.30 ± 0.02	3.92 ± 0.06	-0.1	9.0 ± 0.9
	2.84 ± 0.027[c]	3.95 ± 0.10[c]	(-0.2)[c]	
$[Tb_2(L^{C5})_3]$	0.040 ± 0.003	0.041 ± 0.003	[b]	0.31 ± 0.05
	2.56 ± 0.03[c]	2.70 ± 0.12[c]	(-0.2)[c]	
$[Yb_2(L^{C5})_3]$	$(4.33\pm0.03)\times10^{-3}$	$(47.8\pm0.1)\times10^{-3}$	0.0	0.16 ± 0.02
$[Eu_2(L^{C6})_3]$	0.54 ± 0.02	2.94 ± 0.04	0.1	0.35 ± 0.05
	0.67 ± 0.05[c]	4.12 ± 0.12[c]	(-0.2)[c]	
$[Tb_2(L^{C6})_3]$	$(10.5\pm0.8)\times10^{-3}$	$(9.5\pm0.8)\times10^{-3}$	[b]	[d]
	1.85 ± 0.17	1.94 ± 0.15	(-0.3)[c]	
$[Yb_2(L^{C6})_3]$	$(4.28\pm0.02)\times10^{-3}$	$(49.8\pm0.5)\times10^{-3}$	0.0	0.15 ± 0.02

[a] See text for equations used. [b] Equation not applicable. [c] At 77 K. [d] Too small to be measured.

with the following phenomenological equations [Eqs. (4)–(6)],.[41,42] in which $\Delta k_{obs}=1/\tau(H_2O)-1/\tau(D_2O)$ (in ms^{-1} for Eu^{III} and Tb^{III}, and μs^{-1} for Yb^{III}); the corrective factor takes into account second-sphere effects.

$$q(Eu) = 1.11 \times (\Delta k_{obs} - 0.31) \quad (4)$$

$$q(Tb) = 5.0 \times (\Delta k_{obs} - 0.06) \quad (5)$$

$$q(Yb) = 1.0 \times (\Delta k_{obs} - 0.20) \quad (6)$$

It is important to realise that these equations are only valid if deactivation through O–H vibrations is the main non-radiative deactivation path operating in the studied compound. The accuracy of these equations is usually accepted to be ±0.3 water molecules. All the q values found for the Eu^{III} helicates are close to zero, pointing to the absence of water molecules interacting in the first coordination sphere. The $Eu(^5D_0)$ lifetimes are quite long for the helicates with H_2L^{C4} and H_2L^{C5} and not too temperature-dependent, increasing by about 20% from room temperature to 10 K; this means that vibrational deactivation are minimised in the relatively rigid coordination cavity. The situation for the helicate with H_2L^{C6} is quite different in that the lifetime is short and quite temperature-dependent, both in water and deuterated water. Since the calculated value of q is still zero, this means that another temperature-dependent deactivation mechanism is operating in this compound; back transfer or quenching by a LMCT state are potential candidates, but since no LMCT could be evidenced, the former mechanism is most likely to be the cause of the quenching. In the case of Tb^{III}, the room-temperature lifetime of the $^5D_4$ level is very short, in the range 10–120 μs in water and 10–170 μs in deuterated water; that both sets of data are very similar points to a temperature-dependent mechanism different from O–H quenching operating in the three molecular edifices: the lifetimes at 77 K are indeed much longer, in the millisecond range. Since both 4f–5d[43] or charge-transfer states[44] have too high energy for being involved in such a quenching, we again think that back transfer is the mechanism most likely involved. In such a case, Equation (5) is not applicable for the calculation of q; if one uses this equation with 77 K data, one gets q values close to zero. This has to be used with caution since the procedure is not validated, although it also works for Eu^{III} (Table 5) and sometimes yield values different from zero.[45]

The reasoning about back transfer seems to be further substantiated by the Yb^{III} lifetimes in water, which are almost identical within experimental error for the helicates with H_2L^{C5} and H_2L^{C6}. In these cases, the energy gaps between the $^2F_{5/2}$ level and the ligand triplet states are far too large ($\approx10000\ cm^{-1}$) for back transfer to be operative. As a consequence, the main quenching mechanism occurs through vibrators located in the first- and second-coordination spheres.[46] The lifetimes in deuterated water are consequently about tenfold longer than in water and the calculated q values are zero.

The quantum yields of the metal-centred luminescence upon ligand excitation are also reported in Table 5. The best ligand for sensitising the Eu luminescence is H_2L^{C4}, with an overall quantum yield of 15% down from 21% for $[Eu_2(L^{C2})_3]$.[31] In moving to H_2L^{C5}, the quantum yield further decreases to 9%, while the simple grafting of a methoxy group on the 7-position of the *N*-methyl benzimidazole moiety of H_2L^{C2} to yield H_2L^{C6} is very detrimental for the reasons explained above and the quantum yield is under 1%. With respect to Tb^{III}, none of the three new ligands is adequate for a substantial sensitisation, the quantum yields remaining quite small or even not measurable for H_2L^{C6}; again ligand H_2L^{C4} is the best of the series. The quantum yield of the Yb^{III} helicates seems to be rather insensitive to modification of the ligands, the quantum yield remaining approximately constant (0.15%) for ligands H_2L^{C2}, H_2L^{C5} and H_2L^{C6}. In view of these results, and given our initial goal of shifting the excitation wavelength toward the visible, only $[Eu_2(L^{C5})_3]$ will be tested as luminescent bioprobe.

Cell-imaging properties of $[Eu_2(L^{C5})_3]$: Before starting imaging experiments, we have checked that the growth of HeLa cells is not inhibited by the Eu^{III} chelate. Cell proliferation was determined by the WST-1 assay at time intervals in the range 0.5–24 h for incubation concentrations of the helicate of 0, 125, 250, and 500 μM. The results clearly show no influence of the europium complex on cell proliferation (Figure S10 in the Supporting Information). The viability of the

cells after 24 h incubation with concentrations of the chelate up to 500 μM is also 100±1%, as determined with the same WST-1 assay. Therefore the helicate can be considered as being non-cytotoxic, with $IC_{50} > 500$ μM. In the following experiment, HeLa cells were grown on plastic-bottomed cell culture μ-dishes and incubated with a solution of $[Eu_2(L^{C5})_3]$ in RPMI-1640 (0–100 μM) for 6 h at 37°C. Time-resolved luminescence images recorded with an excitation wavelength of 365 nm and a delay time of 100 μs to eliminate the background fluorescence are shown on Figure 6. Bright spots start to appear in the cytoplasm of the cells for an incubation concentration as low as 5 μM. The uptake of the helicate at an incubation concentration of 200 μM was also followed versus time and emission from the chelate can be detected after only 15 min (Figure 6 and Figure S11 in the Supporting Information).

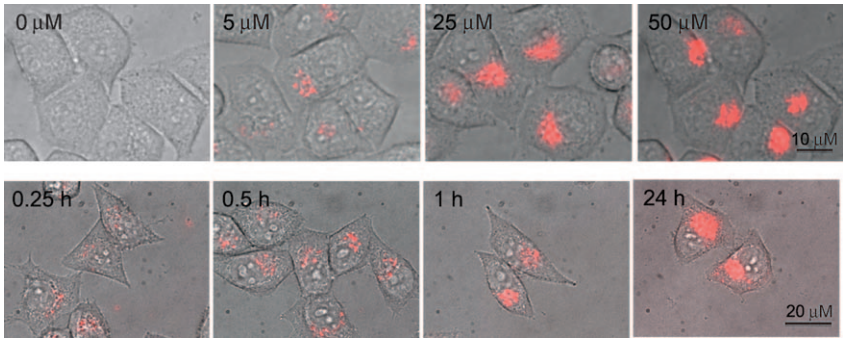

Figure 6. Merged bright-field and time-resolved luminescence microscopy of HeLa cells loaded with $[Eu_2(L^{C5})_3]$. Top row: Cells incubated with various concentrations of $[Eu_2(L^{C5})_3]$ in RPMI-1640 for 6 h at 37°C; conditions: Pan-Fluor lens 40× magnification, 365 nm excitation (BP 80 nm), 420 nm LP emission filter, 100 μs delay, 30 s exposure time. Bottom row: Time-course of the uptake upon incubation at 37°C with $[Eu_2(L^{C5})_3]$ 200 μM; same conditions as above, but for the magnification (100×) and the excitation (340 nm, BP 70 nm).

Given the molecular weight of the helicate (3133 Da), the mechanism of intake is very likely to be endocytosis, as demonstrated for helicates with H_2L^{CX} ($X=2$, $2'$, and 3).[28,32] The microscopy images shown on Figure 6 point to a localisation into endosomes and/or lysosomes. To learn more on this aspect, we performed two co-localisation experiments with organic dyes. The fluorescence of the organic dyes was measured by the conventional mode, while Eu^{III} luminescence was detected in a time-gated mode. In the first experiment, HeLa cells were incubated simultaneously with 100 μM of $[Eu_2(L^{C5})_3]$ and 100 nM of LysoTracker blue DND-22 during 4 h at 37°C. Superimposed images (Figure S12 in the Supporting Information) unmistakably point to the presence of the helicate into secondary endosomes and lysosomes. Secondly, co-localisation experiments were conducted with two organic dyes known to penetrate into the endoplasmatic reticulum (ER) and the Golgi apparatus, respectively. Cells were incubated successively with the Eu^{III} chelate and the two organic trackers. The resulting images are shown on Figure 7 and reveal that the majority of the neutral helicates stain vesicles contained within the endoplasmatic reticulum and not in the Golgi apparatus.

The number of $[Eu_2(L^{C5})_3]$ helicates trapped into HeLa cells was determined by using Delfia® technology. Cells were loaded overnight with the chelate (25 μM) in a 6-well cell cul-

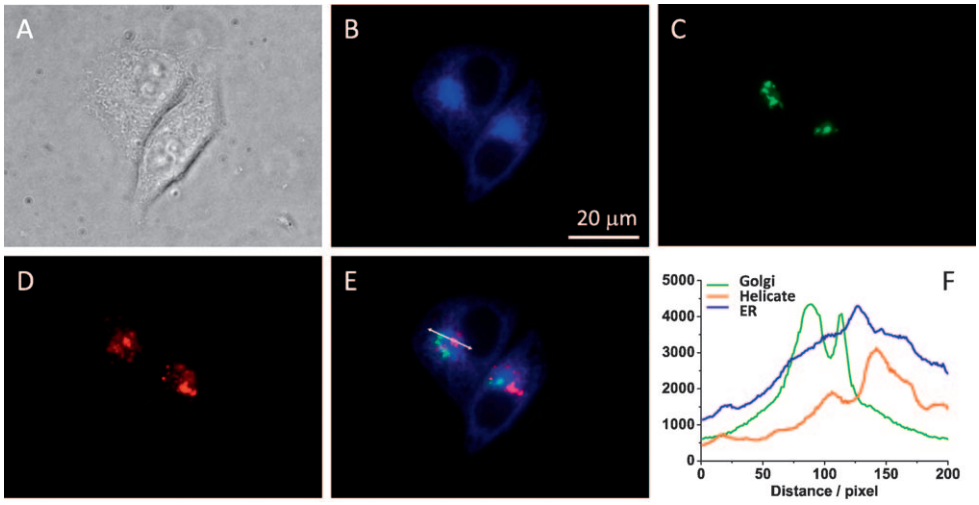

Figure 7. Images of HeLa cells loaded with 100 μM of $[Eu_2(L^{C5})_3]$ for 4 h at 37°C followed by 30 min incubation with 1 μM of ER-tracker Blue-White DPX at 37°C and finally by 30 min incubation at 4°C with 5 μM of Golgi-Tracker BODIPY® FL C_5-ceramide complexed to BSA. A) bright field image. B) fluorescence of ER-Tracker (Plan-fluor lens 100×, 365 nm (BP 80 nm) excitation filter, 450 nm (BP 65 nm) emission filter, 4 s exposure time). C) fluorescence of Golgi-tracker (Plan-fluor lens 100×, 480 nm (BP 30 nm) excitation filter, 530 nm (BP 30 nm) emission filter, 1 s exposure time). D) Eu^{III} luminescence (Plan-fluor lens 100×, 340 nm (BP 70 nm) excitation filter, 420 nm longpass emission filter, 10 μs excitation pulse length, 100 μs delay time, 600 μs gate time, 30 s exposure time). E) merged images. F) Densitometric traces over the path shown in E.

ture plate and harvested by trypsinisation after extensive washing with PBS. The number of labelled cells was estimated by trypan blue staining. The Eu^{III} luminescence was measured in time-gated mode after complete lysis of the cells. In parallel, a standard curve was established by spiking 500 unloaded cells with different concentrations of $[Eu_2(L^{C5})_3]$ and is shown on Figure S13 in the Supporting Information. From the collected data, each cell contains on average 5.2×10^{-16} mol of the $[Eu_2(L^{C5})_3]$ helicate, translating to 3.1×10^8 molecules of chelate per cell, at the low end of the $(3.2–5.4)\times10^8$ range observed for the other helicates.[28,32] This is comparable to the number of macrocyclic complexes per cell found by Parker et al.: 1.2×10^8 to 1.2×10^9.[18,47] The emission spectrum of intracellular $[Eu_2(L^{C5})_3]$ displays an overall shape very similar to the luminescence spectrum in the cell culture medium (Figure S14 in the Supporting Information) and in RPMI-1640, translating into $^5D_0\rightarrow{}^7F_J/^5D_0\rightarrow{}^7F_1$ intensity ratios being alike, within experimental error. The only difference lies in the $^5D_0$ lifetime, which is much shorter in cellulo; since the decay remains perfectly monoexponential, a possible explanation is a quenching by endogenous antioxidants present in the cells.[48]

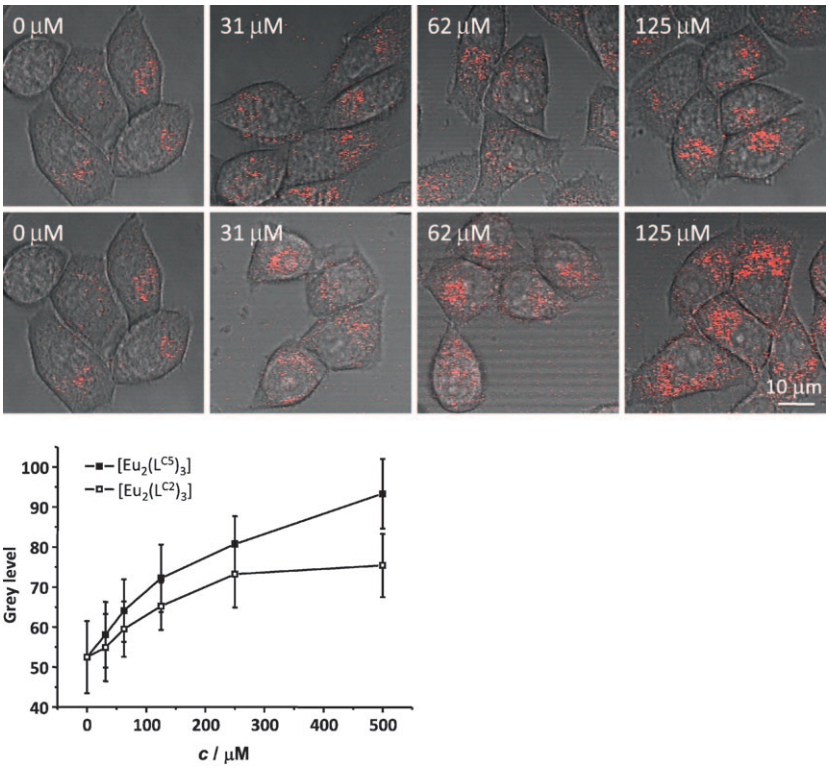

Figure 8. Top: Confocal microscopy images of HeLa cells incubated with different concentrations of $[Eu_2(L^{C2})_3]$ (1st row) and $[Eu_2(L^{C5})_3]$ (2nd row) during 18 h at 37 °C; lens Plan-Apochromat 63/1.30 oil, 405 nm excitation, LP emission filter 505 nm. Bottom: Corresponding luminescence intensity versus incubation concentration.

In view of the above data, $[Eu_2(L^{C5})_3]$ appears to be a suitable luminescent probe for cell imaging and sensing. Compared to $[Eu_2(L^{C2})_3]$, however, its quantum yield is 2.5-fold smaller, which is a handicap. However, when it comes to confocal microscopy, the longer excitation wavelength of this new bioprobe is a definite advantage, since it still absorbs substantially at 405 nm. A comparative study of $[Eu_2(L^{C5})_3]$ versus $[Eu_2(L^{C2})_3]$ conducted on HeLa cells demonstrates the superiority of the former in confocal microscopy (Figure 8 and Figure S15 in the Supporting Information).

Discussion and Conclusion

When it comes to designing luminescent bioprobes it is vital to be able to correlate the structure of the sensitising ligand with the photophysical properties. Theoretical modelling leading to workable structure–property relationships are not yet reliable enough due to the complexity of the ligand-to-lanthanide energy-transfer process,[49] except in some isolated cases.[50,51] In fact, the quantity of interest is the sensitisation efficiency of the ligand, η_{sens}, which can be deduced from two experimentally accessible parameters, the overall quantum yield, that is, the quantum yield of the metal-centred luminescence upon excitation in the ligand electronic levels, and the intrinsic quantum yield, that is, the quantum yield of the metal-centred luminescence upon direct f–f excitation [Eq. (7)].

$$\eta_{sens}=\frac{Q_{Ln}^{L}}{Q_{Ln}^{Ln}}\qquad Q_{Ln}^{Ln}=\frac{\tau_{obs}}{\tau_{rad}} \tag{7}$$

The relationship between the composition of the inner (and partly outer) coordination sphere(s) of the luminescent metal ion and Q_{Ln}^{Ln} is relatively straightforward and well understood in that a large intrinsic quantum yield requires a rigid metal-ion environment devoid of high energy vibrations.[42] On the other hand, the link between η_{sens} and the chemical and electronic structure of the luminescent edifice is much more elaborate. Therefore, a precise determination of this quantity for a series of related compounds certainly helps in understanding this relationship. One difficulty is that it is difficult to measure experimentally, because of the very weak oscillator strength of the f–f transitions, which, in addition, are often overlapped by much stronger ligand ab-

sorptions. A way out is to calculate this quantity with the observed (τ_{obs}) and radiative (τ_{rad}) lifetimes. The latter quantity cannot be measured directly, rather it has to be calculated from Einstein's spontaneous emission coefficients, themselves estimated from the absorption spectrum. The procedure is complex and yields variable results.[52] Fortunately, in the case of Eu^{III}, and thanks to the magnetic dipole nature of the $^5D_0 \rightarrow {}^7F_1$ transition, a simplified equation is at hand [Eq. (8)].[53]

$$\frac{1}{\tau_{rad}} = A_{MD,0} \cdot n^3 \left(\frac{I_{tot}}{I_{MD}} \right) \quad (8)$$

In Equation (8) $A_{MD,0}$, which is the emission probability of the $^5D_0 \rightarrow {}^7F_1$ transition, is independent of the metal-ion environment and is equal to 14.65 s^{-1}; I_{tot} is the experimental total integrated emission intensity ($^5D_0 \rightarrow {}^7F_J$, $J = 0$–6) and I_{MD} the corresponding value for the magnetic dipole transition only. Relevant data for the three Eu^{III} helicates tested here as well as for the four other ones published previously are collected in Table 6. The striking feature is that the radiative lifetime is remarkably constant in this series of compounds. This means that non-radiative deactivation processes are quite comparable in the seven helicates owing to very similar N_6O_3 coordination environments. The intrinsic quantum yield is also very similar for all helicates, but for [$Eu_2(L^{C6})_3$], a logical consequence of the back-transfer mechanism evidenced upon analysis of the temperature dependence of the $^5D_0$ lifetime. On the other hand, the sensitisation efficiency is quite sensitive to substitution of the ligand core. With respect to the reference helicate [$Eu_2(L^{C2})_3$] (58%), η_{sens} decreases by one third to 38% when *N*-pyrazolyl groups are grafted, and by half, to 26%, when the benzimidazole core is modified by fusion of a pyridine moiety. Therefore, the decrease in overall quantum yield for the two new helicates with respect to [$Eu_2(L^{C2})_3$] is entirely due to a less efficient energy transfer. On the other hand, the very poor quantum yield of [$Eu_2(L^{C6})_3$] is due to the conjugated effect of an extremely small sensitisation efficiency of about 4% and of additional non-radiative deactivation due to back transfer.

Table 6. Radiative lifetimes of the Eu($^5D_0$) level and ligand sensitisation parameters for the [$Ln_2(L^{CX})_3$] helicates.

Helicate	τ_{rad} [ms]	Q^{Ln}_{Ln} [%]	η_{sens} [%]	$\Delta E(^3\pi\pi^*-{}^5D_0)$ [cm^{-1}]	Ref.
[$Eu_2(L^{C1})_3$]	6.8±0.3	37±4	67±10	3330	[28]
[$Eu_2(L^{C2})_3$]	6.9±0.3	36±4	58±8	4720	[28]
[$Eu_2(L^{C2'})_3$]	6.6±0.3	37±4	52±7	4570	[32]
[$Eu_2(L^{C3})_3$]	6.2±0.3	36±4	30±5	4820	[28]
[$Eu_2(L^{C4})_3$]	6.4±0.3	40±4	38±6	3710	this work
[$Eu_2(L^{C5})_3$]	6.7±0.2	35±4	26±4	3460	this work
[$Eu_2(L^{C6})_3$]	6.8±0.9	8±1	4.4±0.7	2610	this work

It is common to discuss sensitisation efficiency in terms of the energy gap between the emitting level and the 0–phonon energy of the triplet state. In some instances, correlation has effectively been found, for instance for a series of polyaminocarboxylates[54] or Schiff base complexes,[55] the rule of thumb being that $\Delta E(^3\pi\pi^*-{}^5D_J)$ should be in the range 2500–3500 cm^{-1} for optimum transfer. Examination of the data reported in Table 6 and plotted on Figure 9 clearly demonstrates the insufficiency of such a methodology in that there is no correlation between the relevant photophysical data and the energy gaps for both Eu^{III} and Tb^{III} bimetallic helicates. As we have pointed out previously,[31,45] this simplistic approach does not take into account the overlap integrals between the emission spectrum of the donor and the absorption spectrum of the acceptor, a parameter which is highly sensitive, in the present cases, to the band shape of the triplet emission, which extends far into the visible region.

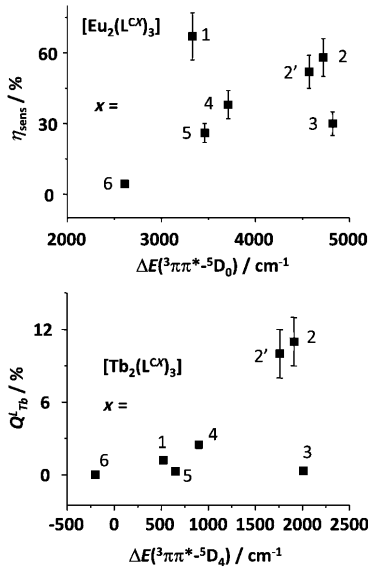

Figure 9. Top: Efficiency of the H_2L^{CX} ligands for the sensitisation of Eu^{III} luminescence versus $\Delta E(^3\pi\pi^*-{}^5D_0)$. Bottom: Overall quantum yields of the [$Tb_2(L^{CX})_3$] helicates versus $\Delta E(^3\pi\pi^*-{}^5D_4)$.

The data reported here for the four new helicates demonstrate that if derivatisation of the ligand core can lead to predicted changes in the energy of the ligand levels, their influence on the photophysical properties is more difficult to prophesy. Moreover they also show the limited range of energy-tuning available when it comes to shifting the excitation wavelength into the visible region, while maintaining the luminescence properties. In this respect, [$Eu_2(L^{C5})_3$] represents a good compromise. Its performances as a cell-imaging stain are satisfying when time-gated microscopy is used, although the expected improvement, with respect to [$Eu_2(L^{C2})_3$], in shifting the excitation wavelength from 330 to 365 nm did not occur, simply because the absorption profile of the former helicate is narrower so that the overlap between the absorption spectra and the excitation bandwidth is very similar for the two helicates. Recently, Parker et al.

have reported an Eu complex derived from the cyclen framework fitted with an azathiaxanthone pendant having an excitation wavelength of 382 nm and a comparable quantum yield to $[Eu_2(L^{C5})_3]$ in water (8.9%);[56] we note, however, that the molar absorption coefficient of the xanthone antenna at the absorption maximum is about tenfold smaller compared to $[Eu_2(L^{C5})_3]$.

On the other hand, when it comes to confocal microscopy, $[Eu_2(L^{C5})_3]$ is largely better than $[Eu_2(L^{C2})_3]$. Since 1) confocal microscopy is widely used in biology, 2) H_2L^{C5} bears the same polyoxyethylene pendant arms as H_2L^{C2}, meaning that further derivatisation is at hand for planning coupling and targeting experiments and 3) its Eu^{III} helicate is non-cytotoxic, $[Eu_2(L^{C5})_3]$ is a potentially valuable bimetallic lanthanide probe, for both time-resolved and confocal microscopy. It localises in secondary endosomes and lysosomes that mainly co-localise with the endoplasmatic reticulum, so that it lends itself to studies on a long timescale, especially that excitation wavelengths less damageable for living cells can be used (e.g., 405 nm).

Experimental Section

Starting materials and general procedures: Chemicals and solvents were purchased from Fluka and Aldrich. Solvents were purified by a non-hazardous procedure by passing them onto activated alumina columns (Innovative Technology Inc. system).[57] Stock solutions of lanthanides were prepared just before use in freshly boiled, doubly distilled water from the corresponding $Ln(ClO_4)_3{\cdot}xH_2O$ salts (Ln = La, Eu, Gd, Tb, Yb, Lu , x = 2.5–4.5). These salts were prepared from their oxides (99.99%, Rhodia Electronic and Catalysis or Research Chemicals, Phoenix, Arizona) in the usual way.[58] Concentrations of the solutions were determined by complexometric titrations using a standardised Na_2H_2EDTA solution in urotropine buffered medium and with xylenol orange as indicator.[59]

Analytical measurements: NMR spectra were measured at 25°C on Bruker Avance DRX 400 (^{1}H, 400 MHz) and AV 600 (^{13}C, 600 MHz), and AV 800 (^{13}C, 800 MHz) spectrometers. Spectra of organic compounds were recorded in $CDCl_3$ (99.8%, Aldrich), MeOD (99.8%, Aldrich), D_2O (99.9%, Aldrich) or [D_6]DMSO (99.8%, Aldrich) and those of the helicates in D_2O (99.9%, Aldrich) and NaOD 0.1 M starting from NaOD 25% from Aldrich (99.5%); deuterated solvents were used as internal standards and chemical shifts are given with respect to TMS. The ESI-MS spectra of the ligands were obtained on a Finningan SSQ 710C spectrometer using 10^{-5}–10^{-4} M solutions in acetonitrile/H_2O/acetic acid (50:50:1), capillary temperature 200°C and acceleration potential 4.5 keV. The instrument was calibrated using the horse myoglobin standard and the analyses were conducted in positive mode. ESI-TOF spectra in positive ion mode were recorded on a Q-TOF Ultima mass spectrometer (Micromass, Manchester, UK) equipped with a Z-spray type ESI source. Phosphoric acid was used for mass calibration in the range 100–2000 m/z. Data were acquired and processed with Masslynx version 4.0. Electrospray conditions were as follows: capillary voltage, 3 kV; source temperature, 80°C; cone voltage, 35 V; source block temperature, 150°C. The ESI nebulisation and drying gas was nitrogen. The sample was introduced through a syringe pump operating at 20 μL min^{-1}. The simulation of spectra was achieved with Molecular Weight Calculator 6.42®; high-resolution spectra of the three ligands are shown in Figure S16 in the Supporting Information. UV/Vis spectra were measured in 0.2 cm quartz Suprasil® cells on a Perkin–Elmer Lambda 900 spectrometer. Molecular modelling was performed with the CAChe® workpackage 7.5 (Fujitsu, 2000–2006). Stability constants were determined by spectrophotometric titration of H_2L^{CX} by Ln^{III} (Ln = La, Eu, Lu) at fixed pH 7.4 (0.1 M Tris-HCl buffer) with the help of a J&M diode array spectrometer (Tidas series) connected to an external computer. All titrations were performed in a thermostated (25.0 ± 0.1°C) glass-jacketed vessel at μ = 0.1 M (KCl). Factor analysis[60] and mathematical treatment of the spectrophotometric data were performed with the Specfit® software.[61] IR spectra were obtained on a Spectrum One Perkin–Elmer FT-IR spectrometer equipped with an ATR accessory. Elemental analyses were performed by Dr. Euro Solari, Elemental Analysis Laboratory of the Institute of Chemical Sciences and Engineering, EPFL.

Luminescence spectra and lifetimes were collected either on a Horiba–Jobin Yvon FL 3–22 fluorimeter or on a home-made high-resolution setup, according to procedures published previously.[62] Quantum yields were measured both by a comparative method with $[Eu_2(L^{C1})_3]$ as standard (Q = 24%)[30] and by an absolute method[63] using a specially designed integration sphere.[64] The two methods gave consistent results, as reported previously.[31]

Synthesis of the intermediates I^{C4a}, I^{C5a} and I^{C5a} (Scheme 4): The synthesis of 4,4′-bis(*N*-methylamino)-5,5′-dinitro-2,2′-bis(*N*-pyrazolyl)diphenylmethane (I^{C4a}) started with a direct C–N coupling of 5-chloro-*N*-methyl-2-nitrobenzeneamine with pyrazole in presence of catalytic amounts of $[Fe^{III}(acac)_3]$ and $Cu^{II}O$, yielding compound **2**. The second step was based on a chemical procedure commonly used in our laboratory.[65]

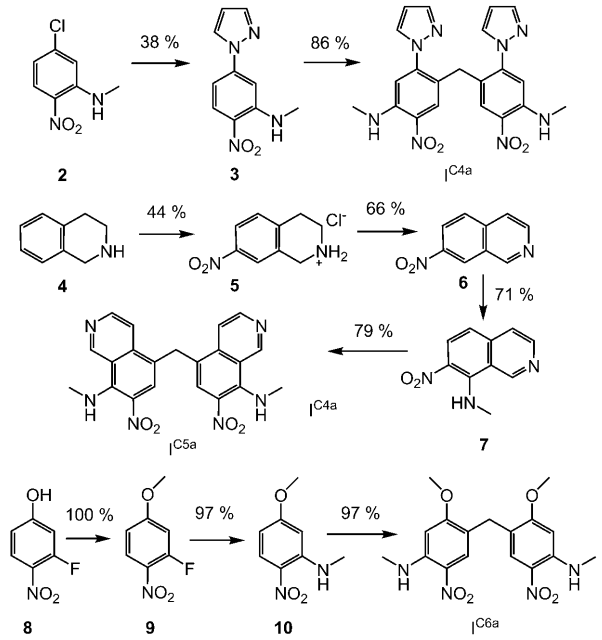

Scheme 4. Synthetic routes to the intermediates I^{C4a}, I^{C5a} and I^{C6a}.

The first step in the synthesis of I^{C5a} consisted of a nitration at the 7-position of 1,2,3,4-tetrahydroisoquinoline in a mixture of H_2SO_4/KNO_3,[66] followed by oxidation into 7-nitroisoquinoline by using an excess of Fremy's salt.[67,68] Despite its drawbacks such as the high cost of the reagent and the long reaction time (7 days), this reaction is the only known way to obtain the target product in absence of impurity; we note that the yield obtained (66%) is better than other published ones, 30%[67] and 55%.[68] The only method we found for incorporating the methylamino group in 8-position of the 7-nitroisoquinoline was by direct methylamination.[69,70] The good selectivity obtained for the first time on a nitroisoquinoline, as well as the substantial yield, can be explained by two factors: 1) the presence of a nitro group at the 7-position, and 2) the strongly electrophilic nature of the carbon atom bearing the incorporated methylamino group. Finally, compound I^{C5a} was obtained similarly to I^{C4a}. The solubility of I^{C5a} was extremely low in all commonly used organic solvent; nevertheless, well-resolved NMR ^{1}H spectra were obtained by dissolution into a mixture of deuterated water containing one drop of DCl (35%).

The first step in the synthesis of I^{C6a} consisted of methylating the phenol function of the commercially available 3-fluoro-4-nitrophenol **8** in presence of an excess of methyl iodide. The resulting 3-fluoro-4-methoxynitrobenzene (**9**) was subsequently converted into 2-*N*-methylamino-4-methoxynitrobenzene (**10**) by aromatic nucleophilic substitution of a fluoride atom by a *N*-methylamino group.[71] Finally, the target compound I^{C6a} was obtained similarly to I^{C4a}. The overall yield of the synthesis was 94%.

***N*-Methyl-2-nitro-4-(1*H*-pyrazol-1-yl)benzeneamine (2)**: A solution of 5-chloro-*N*-methyl-2-nitrobenzeneamine (2.00 g, 10.7 mmol) in DMF (25 mL) was added to a mixture of pyrazole (1.09 g, 16.1 mmol), Cs_2CO_3 (6.98 g, 21.4 mmol), $[Fe(acac)_3]$ (1.26 g, 3.57 mmol) and CuO (0.085 g, 1.08 mmol) under nitrogen. The corresponding mixture was heated to 140°C and stirred for 24 h. After cooling to room temperature, the mixture was diluted with dichloromethane and then filtered. The filtrate was washed twice with water, and the combined aqueous phases were extracted with CH_2Cl_2 (2×250 mL). The organic layers were combined, dried over anhydrous Na_2SO_4 and concentrated to give the crude product, which was further purified by column chromatography (neutral alumina, CH_2Cl_2/hexane 7:3→CH_2Cl_2) to provide **2** as an orange solid (884 mg, 38%). ^{1}H NMR (400 MHz, $CDCl_3$) δ=3.11 (s, 3H; NCH_3), 6.53 (dd, ^3J=2.2 Hz, ^3J=1.8 Hz, 1H; H_{Pyr}), 6.91 (dd, ^3J=9.2 Hz, ^4J=2.2 Hz, 1H; H_{Ph}), 7.31 (d, ^3J=1.8 Hz, 1H; H_{Pyr}), 7.78 (d, ^3J=2.2 Hz, 1H; H_{Pyr}), 8.01 (d, ^4J=2.2 Hz, 1H; H_{Ph}), 8.23 (br s, 1H; NH), 8.28 ppm (d, ^3J=9.2 Hz, 1H; H_{Ph}); ^{13}C NMR (800 MHz, $CDCl_3$): δ=29.90 (NCH_3), 102.00 (CH_{Ph}), 105.46 (CH_{Ph}), 108.91 (CH_{Pyr}), 127.25 ($C_{Ph\,quat}$), 128.97 (CH_{Pyr}), 129.80 ($C_{Ph\,quat}$), 142.44 (CH_{Pyr}), 145.47 ($C_{Ph\,quat}$), 147.49 ppm ($C_{Ph\,quat}$); ESI-MS: *m*/*z* calcd: 219.09 $[M+H]^+$; found: 219.39.

4,4′-Methylenebis[*N*-methyl-2-nitro-5-(1*H*-pyrazol-1-yl)aniline] (I^{C4a}): Compound **2** (800 mg, 3.67 mmol) and *p*-formaldehyde (55 mg, 1.83 mmol) were dissolved in a concentrated hydrochloric acid solution (40 mL, 25%). The mixture was heated and stirred for 16 h. After cooling, the solution was poured into distilled water (about 50 mL) and neutralised with aqueous ammonia (25%) to pH 10. The resulting orange-red precipitate was filtered, washed with water and dried under vacuum. The crude product was then purified by column chromatography (neutral alumina, CH_2Cl_2/hexane 9:1→CH_2Cl_2/MeOH 99:1) to provide I^{C4a} as a red solid (822 mg, 86%). ^{1}H NMR (400 MHz, $CDCl_3$): δ=2.98 (d, *J*=4.7 Hz, 6H; NCH_3), 4.07 (s, 2H; CH_2), 6.40 (dd, ^3J=2.2 Hz, ^3J=1.8 Hz, 2H; H_{Pyr}), 6.71 (s, 2H; H_{Ph}), 7.50 (d, ^3J=1.8 Hz, 2H; H_{Pyr}), 7.67 (s, 2H; H_{Ph}), 7.72 (d, ^3J=2.2 Hz, 2H; H_{Pyr}), 7.96 ppm (br s, 2H; NH); ^{13}C NMR (600 MHz, $CDCl_3$): δ=29.83 (NCH_3), 32.43 (CH_2), 107.43 (CH_{Ph}), 109.91 (CH_{Pyr}), 121.41 (CH_{Ph}), 129.16 ($C_{Ph\,quat}$), 130.25 (CH_{Pyr}), 130.71 ($C_{Ph\,quat}$), 141.49 (CH_{Pyr}), 145.32 ($C_{Ph\,quat}$), 145.88 ppm ($C_{Ph\,quat}$); ESI-MS: *m*/*z* calcd: 449.17 $[M+H]^+$; found: 449.28; elemental analysis calcd (%) for $C_{21}H_{20}N_8O_4\cdot0.5\,MeOH\cdot0.25\,H_2O$: C 55.09, H 4.84, N 23.91; found: C 55.34, H 4.92, N 24.04.

7-Nitrotetrahydroisoquinoline·HCl (5): Compound **4** (10.0 g, 75.0 mmol) was dissolved in concentrated sulfuric acid (37 mL) under cooling. Potassium nitrate (8.15 g, 80.6 mmol) was added in small portions to the stirred solution, the temperature of which was kept below 5°C. The reaction was allowed to stand overnight at room temperature and then the mixture was poured onto ice. The resulting solution was basified with aqueous ammonia (25%) to pH 10. The aqueous phase was extracted with CH_2Cl_2 (5×250 mL). The organic solvent was removed from the combined organic phases, the remaining crude oil was dissolved in ethanol (60 mL) and concentrated hydrochloric acid (10 mL, 37%) was added. After filtration, the precipitate was washed with ethanol (400 mL) and petroleum ether (100 mL). The hydrochloride salt of 7-nitrotetrahydroisoquinoline was recrystallised from methanol to give a white solid (7.10 g., 44% yield). ^{1}H NMR (400 MHz, D_2O): δ=3.26 (t, ^3J=5.9 Hz, 2H; CH_2), 3.60 (t, ^3J=5.9 Hz, 2H; CH_2), 4.51 (s, 2H; CH_2), 7.50 (d, ^3J=8.3 Hz, 1H; H_{Ph}), 8.14 (s, 1H; H_{Ph}), 8.15 ppm (d, ^3J=8.3 Hz, 1H; H_{Ph}); ^{13}C NMR (800 MHz, D_2O): δ=24.78 (CH_2), 41.00 (CH_2), 44.13 (CH_2), 122.09 (CH_{Ph}), 122.73 (CH_{Ph}), 129.20 ($C_{Ph\,quat}$), 130.22 (CH_{Ph}), 139.52 ($C_{Ph\,quat}$), 146.28 ppm ($C_{Ph\,quat}$); ESI-MS: *m*/*z* calcd: 179.08 $[M+H]^+$, 220.11 $[M+CH_3CN+H]^+$; found: 179.33, 220.33.

7-Nitroisoquinoline (6): Potassium nitrosodisulfonate (44.6 g, 166 mmol) in 4% aqueous sodium carbonate solution (670 mL) was added to **5** (3.20 g, 14.9 mmol). The mixture was vigorously stirred at room temperature for 7 days and the reaction mixture was extracted with CH_2Cl_2 (5×250 mL), dried over anhydrous Na_2SO_4 and concentrated under reduced pressure. The residue was purified by column chromatography (neutral alumina, AcOEt/hexane 60:40→80:20) to give 7-nitroisoquinoline as a yellowish solid (1.71 g., 66% yield). ^{1}H NMR (400 MHz, $CDCl_3$): δ=7.78 (d, ^3J=5.6 Hz, 1H; H_{Py}), 7.99 (d, ^3J=8.5 Hz, 1H; H_{Ph}), 8.47 (dd, ^3J=8.5 Hz, ^4J=2.1 Hz, 1H; H_{Ph}), 8.74 (d, ^3J=5.6 Hz, 1H; H_{Py}), 8.94 (d, ^4J=2.1 Hz, 1H; H_{Ph}), 9.47 ppm (s, 1H; H_{Py}); ^{13}C NMR (800 MHz, $CDCl_3$): δ=120.28 (CH_{Py}), 123.72 (CH_{Ph}), 124.42 (CH_{Ph}), 127.18 ($C_{Ph\text{-}Py\,quat}$), 128.53 (CH_{Ph}), 138.15 ($C_{Ph\,quat}$), 146.20 ($C_{Ph\text{-}Py\,quat}$), 146.50 (CH_{Py}), 154.26 ppm (CH_{Py}); ESI-MS: *m*/*z* calcd: 175.05 $[M+H]^+$, 216.08 $[M+CH_3CN+H]^+$; found: 175.32, 216.32.

8-Methylamino-7-nitroisoquinoline (7): Compound **6** (450 mg, 2.59 mmol) was dissolved in liquid methylamine (10–15 mL) at −10°C. After stirring at −7°C for 30 min, $KMnO_4$ (818 mg, 5.17 mmol) was added. The resulting mixture was stirred at this temperature for 4 h. After evaporation of methylamine, distilled water (100 mL) and CH_2Cl_2 (500 mL) were added to the dark residue. This biphasic mixture was vigorously stirred overnight and then the organic phase was isolated. The aqueous phase was extracted with CH_2Cl_2 (2×250 mL) and the organic phases were combined, dried over anhydrous Na_2SO_4 and filtered. After removal of the solvent, the crude product was charged on a chromatography column (silica gel, AcOEt/hexane 70:30→90:10) to give an orange solid (372 mg, 71% yield). ^{1}H NMR (400 MHz, $CDCl_3$): δ=3.64 (d, *J*=5.6 Hz, 3H; NCH_3), 7.02 (d, ^3J=9.2 Hz, 1H; H_{Ph}), 7.57 (d, ^3J=5.5 Hz, 1H; H_{Py}), 8.32 (d, ^3J=9.2 Hz, 1H; H_{Ph}), 8.63 (d, ^3J=5.5 Hz, 1H; H_{Py}), 9.66 (br s, 1H; NH), 9.77 ppm (s, 1H; H_{Py}); ^{13}C NMR (600 MHz, $CDCl_3$): δ=37.64 (NCH_3), 115.26 (CH_{Ph}), 120.56 ($C_{Ph\text{-}Py\,quat}$), 120.79 (CH_{Py}), 126.72 (CH_{Ph}), 129.55 ($C_{Ph\,quat}$), 141.73 ($C_{Ph\,quat}$), 147.12 (CH_{Py}), 149.20 ($C_{Ph\text{-}Py\,quat}$), 151.11 ppm (CH_{Py}); ESI-MS: *m*/*z* calcd: 204.08 $[M+H]^+$, 245.11 $[M+CH_3CN+H]^+$; found: 204.30, 245.31.

5,5′-Methylenebis(*N*-methyl-7-nitro-8-isoquinolinamine) (I^{C5a}): 8-Methylamino-7-nitroisoquinoline (372 mg, 1.83 mmol) and *p*-formaldehyde (27.4 mg, 9.16×10^{-1} mmol) were dissolved in a concentrated hydrochloric acid solution (25%, 10 mL). The mixture was heated at 80°C and stirred for 16 h. After cooling, the solution was poured into distilled water (50 mL) and neutralised with aqueous ammonia (25%) to pH 10. The resulting orange red precipitate was filtered, washed with water (200 mL) and acetone (200 mL), and dried under vacuum (300 mg, 79% yield). ^{1}H NMR (400 MHz, D_2O/DCl): δ=2.53 (s, 6H; NCH_3), 3.47 (s, 2H; CH_2), 6.97 (s, 2H; H_{Ph}), 7.18 (d, ^3J=7.1 Hz, 2H; H_{Py}), 7.52 (d, ^3J=7.1 Hz, 2H; H_{Py}), 8.85 ppm (s, 2H; H_{Py}); ESI-MS: *m*/*z* calcd: 419.15 $[M+H]^+$, 460.18 $[M+CH_3CN+H]^+$; found: 419.34, 460.35.

2-Fluoro-4-methoxynitrobenzene (9): The reaction was carried out under nitrogen in absence of light. Methyl iodide (3.61 g, 25.4 mmol) was added to a suspension of **8** (2.00 g, 12.7 mmol) and K_2CO_3 (3.95 g, 28.6 mmol) in dry acetone (30 mL). The reaction mixture was sonicated for 5 min and then stirred at room temperature for 48 h to give a pale yellow suspension. It was evaporated to dryness and bi-distilled H_2O (20 mL) was added. The aqueous phase was extracted with CH_2Cl_2 (3×100 mL). The organic phases were combined, dried over Na_2SO_4, filtered and evaporated under reduced pressure. The resulting crude product was charged and eluted on a small column (silica gel, CH_2Cl_2) to remove yellow impurities that were left at the top of the column. The resulting white solid was subsequently dried under vacuum (2.18 g, 100%). ^{1}H NMR (400 MHz, $CDCl_3$): δ=3.90 (s, 3H; OCH_3), 6.74 (dd, $^3J_{H\text{-}F}$=14.1 Hz, $^4J_{H\text{-}H}$=2.6 Hz, 1H; H_{Ph}), 6.77 (ddd, $^3J_{H\text{-}H}$=8.8 Hz, $^4J_{H\text{-}H}$=2.6 Hz, $^5J_{H\text{-}F}$=1.0 Hz, 1H; H_{Ph}), 8.10 ppm (t, $^3J_{H\text{-}H}$=$^4J_{H\text{-}F}$=8.8 Hz, 1H; H_{Ph}); ^{13}C NMR (800 MHz, $CDCl_3$): δ=56.32 (OCH_3), 103.23 (CH_{Ph}), 110.37 (CH_{Ph}), 127.91 (CH_{Ph}), 156.85 ($C_{Ph\,quat}$), 158.17 ($C_{Ph\,quat}$), 165.29 ppm ($C_{Ph\,quat}$); ESI-MS: *m*/*z* calcd: 172.04 $[M+H]^+$; found: 172.38.

2-*N*-Methylamino-4-methoxynitrobenzene (10): A 2 M solution of methylamine in THF (8.77 mL, 17.5 mmol) was added dropwise to **9** (1.50 g, 8.77 mmol) and K_2CO_3 (1.33 g, 9.65 mmol) in CH_2Cl_2 (200 mL). This mixture was stirred at room temperature for 24 h and bi-distilled H_2O

(50 mL) was added. The aqueous phase was extracted with CH_2Cl_2 (3× 100 mL). The organic phases were combined, washed with a saturated solution of NH_4Cl (100 mL), dried over Na_2SO_4 and evaporated under reduced pressure. The crude product was triturated in hexane (about 100 mL) and subsequently filtered. The yellow precipitate collected was dried under vacuum (1.54 g, 97% yield). ^{1}H NMR (400 MHz, $CDCl_3$): δ = 3.01 (s, 3H; NHCH_3), 3.88 (s, 3H; OCH_3), 6.13 (d, ^4J = 2.6 Hz, 1H; H_{Ph}), 6.24 (dd, ^3J = 9.5 Hz, ^4J = 2.6 Hz, 1H; H_{Ph}), 8.14 (d, ^3J = 9.5 Hz, 1H; H_{Ph}), 8.29 ppm (br s, 1H; NH); ^{13}C NMR (800 MHz, $CDCl_3$): δ = 29.67 ($NHCH_3$), 55.63 (OCH_3), 94.74 (CH_{Ph}), 104.50 (CH_{Ph}), 126.52 ($C_{Ph\,quat}$), 129.20 (CH_{Ph}), 148.66 ($C_{Ph\,quat}$), 166.03 ppm ($C_{Ph\,quat}$); ESI-MS: *m*/*z* calcd: 183.08 $[M+H]^+$; found: 183.33.

4,4′-Methanediylbis(5-methoxy-*N*-methyl-2-nitroaniline) (I^{C6a}): Compound **10** (1.00 g, 5.49 mmol) and *p*-formaldehyde (82 mg, 2.75 mmol) were dissolved in a concentrated hydrochloric acid solution (30 mL, 25%). This mixture was heated at 80 °C and stirred for 16 h. After cooling, the solution was poured into bi-distilled H_2O (50 mL) and neutralised with aqueous ammonia (25%) to pH 10. The resulting yellow-orange precipitate was filtered and subsequently washed with water (400 mL). After drying under vacuum, the crude product was purified by column chromatography (silica gel; $CH_2Cl_2 \rightarrow CH_2Cl_2$/MeOH 100→98:2) to give the target product as a yellow solid (995 mg, 97% yield). ^{1}H NMR (400 MHz, $CDCl_3$): δ = 3.05 (s, 6H; NCH_3), 3.72 (s, 2H; CH_2), 3.94 (s, 6H; OCH_3), 6.10 (s, 2H; H_{Ph}), 7.97 (s, 2H; H_{Ph}), 8.39 ppm (br s, 2H; NH); ^{13}C NMR (800 MHz, $CDCl_3$): δ = 28.62 (CH_2), 29.76 ($NHCH_3$), 55.79 (OCH_3), 92.60 (CH_{Ph}), 118.01 ($C_{Ph\,quat}$), 125.53 ($C_{Ph\,quat}$), 128.53 (CH_{Ph}), 148.03 ($C_{Ph\,quat}$), 164.59 ppm ($C_{Ph\,quat}$); ESI-MS: *m*/*z* calcd: 377.15 $[M+H]^+$; found: 377.34; elemental analysis calcd (%) for $C_{17}H_{20}N_4O_6$: C 54.25, H 5.36; N 14.89; found: C 54.52, H 5.38, N 14.92.

4-{2-[2-(2-Methoxyethoxy)ethoxy]ethoxy}pyridine-2,6-dicarboxylic acid diethyl ester: 4-Hydroxypyridine-2,6-dicarboxylic acid diethyl ester (1.50 g, 6.27 mmol), tri(ethyleneglycol) monomethyl ether tosylate (2.20 g, 6.90 mmol) and Cs_2CO_3 (3.07 g, 9.41 mmol) were dissolved in anhydrous DMF (5 mL) under inert atmosphere. This mixture was kept at 60 °C for 24 h under vigorous stirring. The solvent was removed under reduced pressure and the residue was redissolved in bi-distilled H_2O (30 mL). The aqueous phase was washed with CH_2Cl_2 (3×250 mL). The organic phases were combined, dried over Na_2SO_4 and evaporated under reduced pressure. The crude product was charged on a chromatography column of silica gel and subsequently eluted with AcOEt. The collected pale yellow oil was dried under vacuum (1.31 g., 55% yield). ^{1}H NMR (400 MHz, $CDCl_3$): δ = 1.48 (t, ^3J = 7.1 Hz, 6H; OCH_2CH_3), 3.40 (s, 3H; OCH_3), 3.56–3.58 (m, 2H; OCH_2), 3.66–3.68 (m, 2H; OCH_2), 3.70–3.72 (m, 2H; OCH_2), 3.75–3.78 (m, 2H; OCH_2), 3.92–3.95 (m, 2H; $PyOCH_2CH_2$), 4.32–4.34 (m, 2H; $PyOCH_2CH_2$), 4.50 (q, ^3J = 7.1 Hz, 4H; OCH_2CH_3), 7.84 ppm (s, 2H; H_{Py}); ^{13}C NMR (600 MHz, $CDCl_3$): δ = 14.15 (OCH_2CH_3), 58.95 (OCH_3), 62.31 (OCH_2CH_3), 70.20 (OCH_2), 70.32 (OCH_2), 70.61 (OCH_2), 70.93 (OCH_2), 71.87 (OCH_2), 77.01 (OCH_2), 114.36 (CH_{Py}), 150.13 ($C_{Py\,quat}$), 164.30 (C=O), 166.74 ppm ($C_{Py\text{-}O\,quat}$); ESI-MS: *m*/*z*: calcd: 518.26 $[M+H]^+$; found: 518.36.

Synthesis of the ligands The numbering of the polyoxyethylene substituents is shown in Scheme 5.

Diethyl 6,6′-(methylenebis{[2-nitro-5-(1*H*-pyrazol-1-yl)-4,1-phenylene](methylcarbamoyl)})bis(4-{2-[2-(2-methoxyethoxy)ethoxy]ethoxy}pyridine-2-carboxylate) (I^{C4b}): A mixture of **1** (894 mg, 2.50 mmol), freshly distilled $SOCl_2$ (2.98 g, 25.0 mmol), and dry DMF (20 μL, 0.25 mmol) were heated under reflux for 120 min in dry CH_2Cl_2 (20 mL) under inert atmosphere. After evaporation and pumping for 2 h, the residual pale yellow oil was redissolved in dry CH_2Cl_2 (20 mL) and NEt_3 (3 mL), and I^{C4a} (432 mg, 9.63×10^{-1} mmol) dissolved in dry CH_2Cl_2 (10 mL) was added dropwise. The solution was refluxed under inert atmosphere for 16 h and evaporated. The brown residue was redissolved in CH_2Cl_2 (100 mL) and washed with half-saturated NH_4Cl (2×100 mL). The combined organic phases were dried over anhydrous Na_2SO_4, evaporated, and the resulting crude solid was purified by column chromatography (silica gel, $CH_2Cl_2 \rightarrow CH_2Cl_2$/MeOH 95:5) to give the disubstituted product I^{C4b} as brown orange oil (473 mg, 44% yield). This product was directly converted into I^{C4c} without further purification. ESI-MS: *m*/*z* calcd: 1127.43 $[M+H]^+$, 564.22 $[M+2H]^+$/2; found: 1127.32, 564.33.

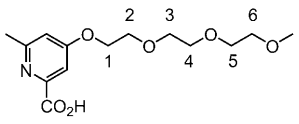

Scheme 5. Numbering used for assigning the NMR spectra.

Diethyl 6,6′-(methylenebis{[1-methyl-6-(1*H*-pyrazol-1-yl)-1*H*-benzimidazole-5,2-diyl]}bis(4-{2-[2-(2-methoxyethoxy)ethoxy]ethoxy}pyridine-2-carboxylate) (I^{C4c}): Freshly activated iron powder (684 mg, 12.3 mmol) and HCl (25%, 3.4 mL) were added to a solution of I^{C4b} (460 mg, 0.408 mmol) in ethanol/water (84/23 mL). The mixture was heated under reflux overnight under inert atmosphere. The solution was cooled, the excess of unreacted iron filtered, and the solvent evaporated. The crude product was redissolved in absolute EtOH (30 mL), conc. H_2SO_4 (97%, 2 mL) was added carefully and the solution was heated under reflux overnight. The solvents were removed after cooling and distilled water (100 mL) was added; the pH was adjusted to 6 with a saturated solution of aqueous $NaHCO_3$. Na_2EDTA (3.04 g, 8.17 mmol) was then added. The colour of the solution turned brown upon addition of H_2O_2 (30%, 1 mL). The pH was then increased to 7 with a saturated solution of aqueous $NaHCO_3$ before extraction with CH_2Cl_2 (2×200 mL). This extraction procedure of the aqueous phase was repeated twice more before combining the organic phases. The latter were extracted again with a saturated solution of aqueous $NaHCO_3$ containing Na_2EDTA (3.04 g); they were finally dried over anhydrous Na_2SO_4, filtered, and evaporated to dryness, which resulted in a brown crude solid which was purified by column chromatography (silica gel; $CH_2Cl_2 \rightarrow CH_2Cl_2$/MeOH 95:5) to give a pale orange solid (192 mg, 46% yield). ^{1}H NMR (400 MHz, $CDCl_3$): δ = 1.45 (t, ^3J = 7.0 Hz, 6H; OCH_2CH_3), 3.36 (s, 6H; OCH_3), 3.52–3.55 (m, 4H; H^6), 3.63–3.66 (m, 4H; H^5), 3.66–3.69 (m, 4H; H^4), 3.73–3.75 (m, 4H; H^3), 3.90–3.92 (m, 4H; H^2), 4.01 (s, 2H; CH_2), 4.33–4.35 (m, 4H; H^1), 4.38 (s, 6H; NCH_3), 4.47 (q, ^3J = 7.0 Hz, 4H; OCH_2CH_3), 6.33 (dd, ^3J = 2.3 Hz, ^3J = 1.8 Hz, 2H; H_{Pyr}), 7.36 (d, ^3J = 1.8 Hz, 2H; H_{Pyr}), 7.42 (s, 2H; H_{Ph}), 7.51 (s, 2H; H_{Ph}), 7.72 (d, ^3J = 2.3 Hz, 2H; H_{Pyr}), 7.96 (d, ^4J = 2.2 Hz, 2H; H_{Py}), 8.07 ppm (d, ^4J = 2.2 Hz, 2H; H_{Py}); ^{13}C NMR (800 MHz, $CDCl_3$): δ = 14.26 (OCH_2CH_3), 33.34 (NCH_3), 33.50 (CH_2), 59.02 (OCH_3), 61.89 (OCH_2CH_3), 68.24 (OCH_2), 69.16 (OCH_2), 70.58 (OCH_2), 70.63 (OCH_2), 70.94 (OCH_2), 71.89 (OCH_2), 106.06 (CH_{Benz}), 108.86 (CH_{Pyr}), 111.97 (CH_{Py}), 113,57 (CH_{Py}), 121.61 (CH_{Benz}), 131.28 (CH_{Pyr}), 131.67 ($C_{Benz\,quat}$), 136.09 ($C_{Benz\,quat}$), 136.19 ($C_{Benz\,quat}$), 140.34 (CH_{Pyr}), 142.35 ($C_{Benz\,quat}$), 148.71 ($C_{Benz\,quat}$), 150.76 ($C_{Py\,quat}$), 151.88 ($C_{Py\,quat}$), 164.78 (C=O), 166.43 ppm ($C_{Py\text{-}O\,quat}$); ESI-MS: *m*/*z* calcd: 1031.46 $[M+H]^+$, 516.23 $[M+2H]^+$/2; found: 1031.30, 516.34.

6,6′-{Methylenebis[1-methyl-6-(1*H*-pyrazol-1-yl)-1*H*-benzimidazole-5,2-diyl]}bis(4-{2-[2-(2-methoxyethoxy)ethoxy]ethoxy}pyridine-2-carboxylic acid) (H_2L^{C4}): Intermediate I^{C4c} (175 mg, 0.172 mmol) was dissolved in absolute EtOH (25 mL) containing NaOH (28.6 mg, 0.714 mmol). This mixture was stirred at room temperature for 2 h. After completion of the reaction, the basic aqueous solution was washed with CH_2Cl_2 (5× 200 mL) then the solution was acidified to pH 2 by addition of HCl (0.02 M). The acidic solution was extracted with CH_2Cl_2 (5×200 mL), dried over anhydrous Na_2SO_4, and evaporated, to give a pale brown solid. This crude product was subsequently purified by column chromatography (silica gel; $CH_3CN \rightarrow CH_3CN/NH_4OH$ 80:20) to give a pale yellow solid (138 mg, 84% yield). ^{1}H NMR (400 MHz, CD_3OD): δ = 3.35 (s, 6H; OCH_3), 3.48–3.51 (m, 4H; H^6), 3.59–3.62 (m, 4H; H^5), 3.63–3.65 (m, 4H; H^4), 3.70–3.72 (m, 4H; H^3), 3.91–3.93 (m, 4H; H^2), 4.11 (s, 2H; CH_2), 4.28 (s, 6H; NCH_3), 4.38–4.40 (m, 4H; H^1), 6.38 (dd, ^3J = 2.0 Hz, ^3J = 1.8 Hz, 2H; H_{Pyr}), 7.35 (s, 2H; H_{Ph}), 7.56 (d, ^3J = 1.8 Hz, 2H; H_{Pyr}), 7.59 (s, 2H; H_{Ph}), 7.68 (d, ^3J = 2.0 Hz, 2H; H_{Pyr}), 7.76 (d, ^4J = 2.0 Hz, 2H; H_{Py}), 7.91 ppm (d, ^4J = 2.0 Hz, 2H; H_{Py}); ^{13}C NMR (600 MHz, CD_3OD): δ = 33.67 (NCH_3), 35.06 (CH_2), 59.08 (OCH_3), 69.53 (OCH_2), 70.34 (OCH_2), 71.40 (OCH_2), 71.58 (OCH_2), 71.83 (OCH_2), 72.94 (OCH_2), 107.44 (CH_{Benz}), 110.94 (CH_{Pyr}), 113.53 (CH_{Py}), 113,93 (CH_{Py}), 121.70 (CH_{Benz}), 133.39 (CH_{Pyr}), 133.48 ($C_{Benz\,quat}$), 136.96 ($C_{Benz\,quat}$), 137.21 ($C_{Benz\,quat}$), 141.39 (CH_{Pyr}), 142.95 ($C_{Benz\,quat}$), 151.77 ($C_{Py\,quat}$), 152.34

($C_{Benzquat}$), 152.93 (C_{Pyquat}), 168.26 ($C_{Py\text{-}Oquat}$), 168.47 ppm (C=O); ESI-MS: *m*/*z* calcd: 975.40 $[M+H]^+$, 488.20 $[M+2H]^+/2$; found: 975.39 (high resolution), 488.38; elemental analysis calcd (%) for $C_{49}H_{54}N_{10}O_{12}\cdot 0.25\,NH_4OH\cdot 1.5\,H_2O$: C 58.22, H 5.80, N 14.20; found: C 58.19, H 5.59, N 14.25.

Diethyl 6,6′-{methylenebis[(7-nitro-5,8-isoquinolinediyl)(methylcarbamoyl)]}bis(4-{2-[2-(2-methoxyethoxy)ethoxy]ethoxy}-2-pyridine carboxylate) (I^{C5b}): A mixture of **1** (700 mg, 1.96 mmol), freshly distilled $SOCl_2$ (2.33 g, 19.6 mmol), and dry DMF (20 μL, 0.250 mmol) were heated under reflux for 120 min in dry CH_2Cl_2 (25 mL) under inert atmosphere. After evaporation and pumping for 2 h, the pale yellow oil formed was redissolved in dry CH_2Cl_2 (50 mL) and NEt_3 (3 mL). Then, I^{C5a} (300 mg, 0.717 mmol) was added in small portions over a period of 1 h. The solution was heated under reflux under an inert atmosphere for 24 h. and evaporated. The brown residue was redissolved in CH_2Cl_2 (100 mL) and washed with half-saturated NH_4Cl (2×100 mL). The combined organic phase were dried over anhydrous Na_2SO_4, evaporated, and the resulting crude solid was purified by column chromatography (silica gel, $CH_2Cl_2\rightarrow CH_2Cl_2$/MeOH 98:2→95:5) to give the disubstituted product I^{C5b} as brown orange oil (364 mg, 47% yield). This product was directly converted into I^{C5c} without further purification. ESI-MS: *m*/*z* calcd: 1097.41 $[M+H]^+$, 549.71 $[M+2H]^+/2$; found: 1097.39, 549.37.

Diethyl (6,6′-[methylenebis(1-methyl-1*H*-imidazo[4,r5-*h*]isoquinoline-5,2-diyl)]bis(4-{2-[2-(2-methoxyethoxy)ethoxy]ethoxy}-2-pyridine carboxylate) (I^{C5c}): Freshly activated iron powder (550 mg, 9.85 mmol) and HCl solution (25%, 2.7 mL) were added to a solution of I^{C5b} (460 mg, 0.408 mmol) in ethanol/water (66/18 mL). The mixture was heated under reflux overnight under an inert atmosphere. The solution was cooled, the excess of unreacted iron filtered and the solvent evaporated. The crude product was redissolved in absolute EtOH (30 mL); H_2SO_4 (97%, 2 mL) was added carefully and the solution was heated under reflux overnight. It was cooled and the solvents were removed. Distilled water (100 mL) was added and the pH was adjusted to 6 with a saturated solution of aqueous $NaHCO_3$; Na_2EDTA (2.44 g, 6.57 mmol) was added to this solution. The colour turned to brown upon addition of H_2O_2 solution (30%, 1 mL). The pH was adjusted to 7 with a saturated solution of aqueous $NaHCO_3$ before extraction with CH_2Cl_2 (5×250 mL). The organic phases were combined, and extracted again with a saturated solution of aqueous $NaHCO_3$ containing Na_2EDTA (2.44 g), dried over anhydrous Na_2SO_4, filtered and evaporated to dryness, which resulted in a brown crude solid subsequently purified by column chromatography (silica gel; $CH_2Cl_2\rightarrow CH_2Cl_2$/MeOH 95:5) to give a pale orange solid (54 mg, 17% yield). ^{1}H NMR (400 MHz, $CDCl_3$): $\delta=1.51$ (t, $^3J=7.1$ Hz, 6H; OCH_2CH_3), 3.38 (s, 6H; OCH_3), 3.54–3.56 (m, 4H; H^6), 3.64–3.67 (m, 4H; H^5), 3.67–3.70 (m, 4H; H^4), 3.73–3.76 (m, 4H; H^3), 3.90–3.93 (m, 4H; H^2), 4.33–4.36 (m, 4H; H^1), 4.53 (q, $^3J=7.1$ Hz, 4H; OCH_2CH_3), 4.98 (s, 6H; NCH_3), 5.00 (s, 2H; CH_2), 7.76 (d, $^4J=2.6$ Hz, 2H; H_{Py}), 7.77 (s, 2H; H_{Isoqu}), 8.01 (d, $^3J=5.4$ Hz, 2H; H_{Isoqu}), 8.02 (d, $^4J=2.6$ Hz, 2H; H_{Py}), 8.66 (d, $^3J=5.4$ Hz, 2H; H_{Isoqu}), 10.12 ppm (s, 2H; H_{Isoqu}); ^{13}C NMR (400 MHz, $CDCl_3$): $\delta=17.41$ (OCH_2CH_3), 39.19 (NCH_3), 40.19 (CH_2), 58.40 (OCH_3), 62.06 (OCH_2CH_3), 68.60 (OCH_2), 69.20 (OCH_2), 70.52 (OCH_2), 71.46 (OCH_2), 71.96 (OCH_2), 72.89 (OCH_2), 116.11 (CH_{Py}), 117.80 (CH_{Py}), 121.45 (CH_{Isoqu}), 123.03 ($C_{Isoqu\,quat}$), 128.73 ($C_{Isoqu\,quat}$), 130.34 ($C_{Isoqu\,quat}$), 133.80 (CH_{Isoqu}), 137.62 ($C_{Isoqu\,quat}$), 144.32 (CH_{Isoqu}), 145.70 ($C_{Isoqu\,quat}$), 147.49 ($C_{Benzquat}$), 148.18 (C_{Pyquat}), 149.95 (C_{Pyquat}), 153.05 (CH_{Isoqu}), 168.50 (C=O), 170.29 ppm ($C_{Py\text{-}Oquat}$); ESI-MS: *m*/*z* calcd: 1001.44 $[M+H]^+$, 501.22 $[M+2H]^+/2$; found: 1001.35, 501.80.

6,6′-[Methylenebis(1-methyl-1*H*-imidazo[4,5-*h*]isoquinoline-5,2-diyl]-bis(4-{2-[2-(2-methoxyethoxy)ethoxy]ethoxy}-2-pyridine carboxylic acid) (H_2L^{C5}): An amount of I^{C5c} (54 mg, 0.0540 mmol) was dissolved in absolute EtOH/H_2O (8/3 mL) containing NaOH (9.1 mg, 0.227 mmol). This mixture was stirred at room temperature for 2 h. After completion of the reaction, the solvents were removed under reduced pressure. The crude product was subsequently purified by column chromatography (silica gel; CH_3CN/NH_4OH 75:25) to give a pale yellow solid (49 mg, 94% yield). ^{1}H NMR (400 MHz, [D_6]DMSO): $\delta=3.18$ (s, 6H; OCH_3), 3.35–3.38 (m, 4H; H^6), 3.46–3.48 (m, 4H; H^5), 3.49–3.51 (m, 4H; H^4), 3.56–3.59 (m, 4H; H^3), 3.76–3.78 (m, 4H; H^2), 4.33–4.35 (m, 4H; H^1), 4.91 (s, 6H; NCH_3), 5.07 (s, 2H; CH_2), 7.65 (s, H, H_{Isoqu}), 7.66 (d, $^4J=2.2$ Hz, 2H; H_{Py}), 7.95 (d, $^4J=2.2$ Hz, 2H; H_{Py}), 8.13 (d, $^3J=5.7$ Hz, 2H; H_{Isoqu}), 8.65 (d, $^3J=5.7$ Hz, 2H; H_{Isoqu}), 10.12 ppm (s, 2H; H_{Isoqu}); ^{13}C NMR (600 MHz, [D_6]DMSO): $\delta=36.72$ (NCH_3), 40.03 (CH_2), 58.06 (OCH_3), 68.16 (OCH_2), 68.53 (OCH_2), 69.64 (OCH_2), 69.81 (OCH_2), 70.04 (OCH_2), 71.29 (OCH_2), 112.28 (CH_{Py}), 112.57 (CH_{Py}), 118.61 (CH_{Isoqu}), 118,74 ($C_{Isoqu\,quat}$), 124.77 ($C_{Isoqu\,quat}$), 129.55 ($C_{Isoqu\,quat}$), 130.70 (CH_{Isoqu}), 133.08 ($C_{Isoqu\,quat}$), 139.95 (CH_{Isoqu}), 142.74 ($C_{Isoqu\,quat}$), 145.76 ($C_{Benzquat}$), 148.54 (C_{Pyquat}), 149.41 (C_{Pyquat}), 151.43 (CH_{Isoqu}), 165.83 ($C_{Py\text{-}Oquat}$), 166.11 ppm (C=O); ESI-MS: *m*/*z* calcd: 945.38 $[M+H]^+$, 473.19 $[M+2H]^+/2$; found: 945.38 (high resolution), 473.20; elemental analysis calcd (%) for $C_{49}H_{52}N_8O_{12}\cdot 0.6\,NH_4OH\cdot 1.5\,NaCl$: C 55.89, H 5.26, N 11.43; found: C 55.94, H 5.25, N 11.30.

Diethyl 6,6′-{methylanediylbis[(5-methoxy-2-nitrobenzene-4,1-diyl)(methylcarbamoyl)]}bis(4-{2-[2-(2-methoxyethoxy)ethoxy]ethoxy}-2-pyridine carboxylate) (I^{C6b}): A mixture of **1** (730 mg, 2.04 mmol), freshly distilled $SOCl_2$ (2.43 g, 20.4 mmol), and dry DMF (20 μL, 0.250 mmol) were heated under reflux for 2 h in dry CH_2Cl_2 (25 mL) under an inert atmosphere. Upon evaporation and pumping for 2 h, the pale yellow oil formed was redissolved in dry CH_2Cl_2 (50 mL) and NEt_3 (3 mL). Then, I^{C6a} (300 mg, 0.717 mmol) was added in small portions over a period of one hour. The solution was heated under reflux under an inert atmosphere for 16 h and evaporated. The brown residue was redissolved in CH_2Cl_2 (100 mL) and washed with half-saturated NH_4Cl (2×100 mL). The combined organic phases were dried over anhydrous Na_2SO_4, evaporated, and the resulting crude solid was purified by column chromatography (silica gel, $CH_2Cl_2\rightarrow CH_2Cl_2$/MeOH 100:0→97:3) to give the disubstituted product I^{C6b} as brown orange oil (654 mg, 79% yield), which was directly converted into I^{C6c} without further purification. ESI-MS: *m*/*z* calcd: 1055.41 $[M+H]^+$, 528.21 $[M+2H]^+/2$; found: 1055.83, 528.34.

Diethyl 6,6′-[methanediylbis(6-methoxy-1-methyl-1*H*-benzimidazole-5,2-diyl)]bis(4-{2-[2-(2-methoxyethoxy)ethoxy]ethoxy}pyridine-2-carboxylate) (I^{C6c}): Freshly activated iron powder (1.04 g, 18.61 mmol) and HCl (25%, 5.2 mL) were added to a solution of I^{C6b} (654 mg, 0.620 mmol) in ethanol/water (128/35 mL). The mixture was heated under reflux overnight under an inert atmosphere. The solution was cooled, the excess of unreacted iron filtered and the solvents evaporated. The crude product was redissolved in absolute EtOH (30 mL); H_2SO_4 (97%, 2 mL) was added carefully and the solution was refluxed overnight. The solvents were removed after cooling and distilled water (100 mL) was added; the pH was then adjusted to 6 with a saturated solution of aqueous $NaHCO_3$; Na_2EDTA (4.62 g, 12.41 mmol) was added to this solution. The colour turned to brown upon addition of H_2O_2 solution (30%, 2 mL). The pH was then increased to 7 with a saturated solution of aqueous $NaHCO_3$ before extraction with CH_2Cl_2 (5×250 mL). The organic phases were combined, and extracted again with a saturated solution of aqueous $NaHCO_3$ containing Na_2EDTA (4.62 g), dried over anhydrous Na_2SO_4, filtered and evaporated to dryness, which resulted in a brown crude solid subsequently purified by column chromatography (silica gel; $CH_2Cl_2\rightarrow CH_2Cl_2$/MeOH 95:5) to give a pale yellow solid (501 mg, 85% yield). ^{1}H NMR (400 MHz, $CDCl_3$): $\delta=1.44$ (t, $^3J=7.0$ Hz, 6H; OCH_2CH_3), 3.35 (s, 6H; OCH_3), 3.52–3.54 (m, 4H; H^6), 3.63–3.65 (m, 4H; H^5), 3.66–3.68 (m, 4H; H^4), 3.72–3.74 (m, 4H; H^3), 3.88–3.90 (m, 4H; H^2), 3.93 (s, 6H; OCH_3), 4.16 (brs, 2H; CH_2), 4.30–4.33 (m, 4H; H^1), 4.36 (s, 6H; NCH_3), 4.45 (q, $^3J=7.0$ Hz, 4H; OCH_2CH_3), 6.81 (s, 2H; H_{Benz}), 7.47 (s, 2H; H_{Benz}), 7.65 (d, $^4J=2.4$ Hz, 2H; H_{Py}), 8.00 ppm (d, $^4J=2.4$ Hz, 2H; H_{Py}); ^{13}C NMR (800 MHz, $CDCl_3$): $\delta=14.60$ (OCH_2CH_3), 31.45 (CH_2), 33.31 (NCH_3), 56.19 (OCH_3), 59.35 (OCH_3), 62.11 (OCH_2CH_3), 68.48 (OCH_2), 69.53 (OCH_2), 70.90 (OCH_2), 70.95 (OCH_2), 71.25 (OCH_2), 72.23 (OCH_2), 91.30 (CH_{Benz}), 111.46 (CH_{Py}), 113.46 (CH_{Py}), 121.39 (CH_{Benz}), 126.90 ($C_{Benzquat}$), 136.61 ($C_{Benzquat}$), 136.98 ($C_{Benzquat}$), 148.05 ($C_{Benzquat}$), 148.79 (C_{Pyquat}), 152.78 (C_{Pyquat}), 156.35 ($C_{Benzquat}$), 165.31 (C=O), 166.58 ppm ($C_{Py\text{-}Oquat}$); ESI-MS: *m*/*z* calcd: 959.44 $[M+H]^+$, 480.22 $[M+2H]^+/2$; found: 959.84, 480.38.

6,6′-[Methanediylbis(6-methoxy-1-methyl-1*H*-benzimidazole-5,2-diyl)]-bis(4-{2-[2-(2-methoxyethoxy)ethoxy]ethoxy}pyridine-2-carboxylic acid) (H_2L^{C6}): Intermediate I^{C6c} (501 mg, 0.523 mmol) was dissolved in absolute EtOH/H_2O (30 mL) containing NaOH (72 mg, 1.80 mmol). This mixture

was kept at 60 °C for 16 h. After completion of the reaction, the solvents were removed under reduced pressure. The residue was dissolved in bi-distilled H_2O (20 mL) and the resulting aqueous solution was acidified to pH 2 by addition of a hydrochloric acid solution 0.02 M. The acidic solution was then extracted with CH_2Cl_2 (5×100 mL), dried over anhydrous Na_2SO_4 and evaporated. The crude product was subsequently purified by column chromatography (silica gel; $CH_3CN \rightarrow CH_3CN/NH_4OH$ 70:30) to give a pale yellow solid (345 mg, 73% yield). ^{1}H NMR (400 MHz, [D$_6$]DMSO): $\delta = 3.21$ (s, 6H; OCH_3), 3.37–3.39 (m, 4H; H^6), 3.47–3.50 (m, 4H; H^5), 3.52–3.53 (m, 4H; H^4), 3.58–3.60 (m, 4H; H^3), 3.78–3.80 (m, 4H; H^2), 3.93 (s, 6H; OCH_3), 4.07 (br s, 2H; CH_2), 4.35 (s, 6H; NCH_3), 4.33–4.35 (m, 4H; H^1), 7.25 (s, 2H; H_{Benz}), 7.25 (s, 2H; H_{Benz}), 7.59 (d, $^4J = 2.2$ Hz, 2H; H_{Py}), 7.93 ppm (d, $^4J = 2.2$ Hz, 2H; H_{Py}); ^{13}C NMR (800 MHz, [D$_6$]DMSO): $\delta = 31.04$ (CH_2), 33.25 (NCH_3), 56.38 (OCH_3), 58.50 (OCH_3), 68.46 (OCH_2), 68.97 (OCH_2), 70.04 (OCH_2), 70.21 (OCH_2), 70.45 (OCH_2), 71.54 (OCH_2), 92.93 (CH_{Benz}), 111.24 (CH_{Py}), 112.77 (CH_{Py}), 120,43 (CH_{Benz}), 125.92 ($C_{Benz\,quat}$), 136.26 ($C_{Benz\,quat}$), 137.04 ($C_{Benz\,quat}$), 147.83 ($C_{Benz\,quat}$), 150.02 ($C_{Py\,quat}$), 152.21 ($C_{Py\,quat}$), 155.69 ($C_{Benz\,quat}$), 166.11 ($C_{Py\text{-}O\,quat}$), 166.37 ppm (C=O); ESI-MS: m/z calcd: 903.38 $[M+H]^+$, 452.19 $[M+2H]^+/2$; found: 903.37 (high resolution), 452.30; elemental analysis calcd (%) for $C_{45}H_{54}N_6O_{14}\cdot H_2O$: C 58.74, H 6.13, N 9.13; found: C 58.47, H 6.14, N 9.14.

Cell imaging experiments and analyses: These experiments have been conducted as previously described.[31,33] A detailed account is given in the Supporting Information.

Acknowledgements

This work is supported through grants from the Swiss National Science Foundation (200020 119866/1) and the Swiss Office for Science and Education within the COST action D38 of the European Science Foundation (contract C07.0107).

[1] J.-C. G. Bünzli, *Acc. Chem. Res.* **2006**, *39*, 53–61.
[2] J.-C. G. Bünzli, C. Piguet, *Chem. Soc. Rev.* **2005**, *34*, 1048–1077.
[3] I. Hemmilä, V. M. Mukkala, *Crit. Rev. Clin. Lab. Sci.* **2001**, *38*, 441–519.
[4] I. Hemmilä, T. Ståhlberg, P. Mottram, *Bioanalytical Applications of Labelling Technologies*, Wallac Oy, Turku, **1995**.
[5] "Lanthanide Chelates as Luminescent Labels in Biomedical Analyses": T. Nishioka, K. Fukui, K. Matsumoto in *Handbook on the Physics and Chemistry of Rare Earths, Vol. 37* (Eds.: K. A. Gschneidner, Jr., J.-C. G. Bünzli, V. K. Pecharsky), Elsevier Science, Amsterdam, **2007**.
[6] V. Laitala, A. Ylikoski, H. M. Raussi, P. Ollikka, I. Hemmila, *Anal. Biochem.* **2007**, *361*, 126–131.
[7] T. Nishioka, J. Yuan, Y. Yamamoto, K. Sumitomo, Z. Wang, K. Hashino, C. Hosoya, K. Ikawa, G. Wang, K. Matsumoto, *Inorg. Chem.* **2006**, *45*, 4088–4096.
[8] P. R. Selvin, *Annu. Rev. Biophys. Biomol. Struct.* **2002**, *31*, 275–302.
[9] C. M. Spangler, C. Spangler, M. Schaerling, *Ann. N. Y. Acad. Sci.* **2008**, *1130*, 138–148.
[10] "Responsive Luminescent Lanthanide Complexes": D. Parker, J. A. G. Williams in *Metal Ions in Biological Systems, Vol. 40* (Eds.: A. Sigel, H. Sigel), Marcel Dekker, New York, **2003**.
[11] P. R. Selvin, *Nat. Struct. Biol.* **2000**, *7*, 730–734.
[12] L. J. Charbonniere, N. Hildebrandt, *Eur. J. Inorg. Chem.* **2008**, 3241–3251.
[13] K. Do, F. C. Muller, G. Muller, *J. Phys. Chem. A* **2008**, *112*, 6789–6793.
[14] W. L. Scaff, D. L. Dyer, K. Mori, *J. Bacteriol.* **1969**, *98*, 246–248.
[15] S. Phimphivong, S. Kolchens, P. L. Edmiston, S. S. Saavedra, *Anal. Chim. Acta* **1995**, *307*, 403–417.
[16] M. P. Houlne, T. S. Agent, G. E. Kiefer, K. Mcmilian, D. J. Bornhop, *Appl. Spectrosc.* **1996**, *50*, 1221–1228.
[17] D. J. Bornhop, D. S. Hubbard, M. P. Houlne, C. Adair, G. E. Kiefer, B. C. Pence, D. L. Morgan, *Anal. Chem.* **1999**, *71*, 2607–2615.
[18] J. H. Yu, D. Parker, R. Pal, R. A. Poole, M. J. Cann, *J. Am. Chem. Soc.* **2006**, *128*, 2294–2299.
[19] A. Beeby, S. W. Botchway, I. M. Clarkson, S. Faulkner, A. W. Parker, D. Parker, J. A. G. Williams, *J. Photochem. Photobiol. B* **2000**, *57*, 83–89.
[20] R. E. Connally, J. A. Piper, *Ann. N. Y. Acad. Sci.* **2008**, *1130*, 106–116.
[21] J. P. Leonard, C. B. Nolan, F. Stomeo, T. Gunnlaugsson, *Top. Curr. Chem.* **2007**, *281*, 1–43.
[22] D. E. Koshland Jr., *Angew. Chem.* **1994**, *106*, 2468–2472; *Angew. Chem. Int. Ed. Engl.* **1994**, *33*, 2375–2378.
[23] J.-M. Lehn, *Proc. Natl. Acad. Sci. USA* **2002**, *99*, 4763–4768.
[24] J.-C. G. Bünzli, C. Piguet, *Chem. Rev.* **2002**, *102*, 1897–1928.
[25] M. Elhabiri, R. Scopelliti, J.-C. G. Bünzli, C. Piguet, *J. Am. Chem. Soc.* **1999**, *121*, 10747–10762.
[26] T. B. Jensen, R. Scopelliti, J.-C. G. Bünzli, *Dalton Trans.* **2008**, 1027–1036.
[27] L. J. Martin, M. J. Hahnke, M. Nitz, J. Wohnert, N. R. Silvaggi, K. N. Allen, H. Schwalbe, B. Imperiali, *J. Am. Chem. Soc.* **2007**, *129*, 7106–7113.
[28] J.-C. G. Bünzli, A.-S. Chauvin, C. D. B. Vandevyver, B. Song, S. Comby, *Ann. N. Y. Acad. Sci.* **2008**, *1130*, 97–105.
[29] C. D. B. Vandevyver, A.-S. Chauvin, S. Comby, J.-C. G. Bünzli, *Chem. Commun.* **2007**, 1716–1718.
[30] A.-S. Chauvin, S. Comby, B. Song, C. D. B. Vandevyver, J.-C. G. Bünzli, *Chem. Eur. J.* **2007**, *13*, 9515–9526.
[31] A.-S. Chauvin, S. Comby, B. Song, C. D. B. Vandevyver, J.-C. G. Bünzli, *Chem. Eur. J.* **2008**, *14*, 1726–1739.
[32] E. Deiters, B. Song, A.-S. Chauvin, C. D. B. Vandevyver, J.-C. G. Bünzli, *New J. Chem.* **2008**, *32*, 1140–1152.
[33] B. Song, C. D. B. Vandevyver, A.-S. Chauvin, J.-C. G. Bünzli, *Org. Biomol. Chem.* **2008**, *6*, 4125–4133.
[34] B. Song, C. D. B. Vandevyver, E. Deiters, A.-S. Chauvin, I. A. Hemmila, J.-C. G. Bünzli, *Analyst* **2008**, *133*, 1749–1756.
[35] M. A. Phillips, *J. Chem. Soc.* **1928**, 172–177.
[36] M. Elhabiri, J. Hamacek, J.-C. G. Bünzli, A.-M. Albrecht-Gary, *Eur. J. Inorg. Chem.* **2004**, 51–62.
[37] J.-C. G. Bünzli, G.-O. Pradervand, *J. Chem. Phys.* **1986**, *85*, 2489–2497.
[38] S. T. Frey, W. d. Horrocks Jr. , *Inorg. Chim. Acta* **1995**, *229*, 383–390.
[39] S. Tobita, M. Arakawa, I. Tanaka, *J. Phys. Chem.* **1985**, *89*, 5649–5654.
[40] J.-C. G. Bünzli, B. Klein, D. Wessner, N. W. Alcock, *Inorg. Chim. Acta* **1982**, *59*, 269–274.
[41] R. M. Supkowski, W. d. Horrocks Jr. , *Inorg. Chim. Acta* **2002**, *340*, 44–48.
[42] A. Beeby, I. M. Clarkson, R. S. Dickins, S. Faulkner, D. Parker, L. Royle, A. S. de Sousa, J. A. G. Williams, M. Woods, *J. Chem. Soc. Perkin Trans. 2* **1999**, 493–503.
[43] P. Dorenbos, *J. Lumin.* **2000**, *91*, 91–106.
[44] S. Shionoya, W. M. Yen, in *Phosphor Handbook* (Eds.: S. Shionoya, W. M. Yen), CRC, Boca Raton, FL (USA), **1999**, Chapter 3, pp. 177–230.
[45] A.-L. Gassner, C. Duhot, J.-C. G. Bünzli, A.-S. Chauvin, *Inorg. Chem.* **2008**, *47*, 7802–7812.
[46] "Lanthanide Near-Infrared Luminescence in Molecular Probes and Devices": S. Comby, J.-C. G. Bünzli, *Handbook on the Physics and Chemistry of Rare Earths, Vol. 37* (Eds.: K. A. Gschneidner, Jr., J.-C. G. Bünzli, V. K. Pecharsky), Elsevier Science, Amsterdam, **2007**, Chapter 235.
[47] F. Kielar, G. L. Law, E. J. New, D. Parker, *Org. Biomol. Chem.* **2008**, *6*, 2256–2258.
[48] R. A. Poole, C. P. Montgomery, E. J. New, A. Congreve, D. Parker, M. Botta, *Org. Biomol. Chem.* **2007**, *5*, 2055–2062.

[49] G. F. de Sá, O. L. Malta, C. D. Donega, A. M. Simas, R. L. Longo, P. A. Santa-Cruz, E. F. da Silva, *Coord. Chem. Rev.* **2000**, *196*, 165–195.
[50] W. M. Faustino, G. B. Rocha, F. R. G. E. Silva, O. L. Malta, G. F. de Sá, A. M. Simas, *THEOCHEM* **2000**, *527*, 245–251.
[51] F. R. Gonçalves e Silva, O. L. Malta, C. Reinhard, H. U. Güdel, C. Piguet, J. E. Moser, J.-C. G. Bünzli, *J. Phys. Chem. A* **2002**, *106*, 1670–1677.
[52] A.Aebischer, F.Gumy, J.-C. G.Bünzli, unpublished work, **2008**.
[53] M. H. V. Werts, R. T. F. Jukes, J. W. Verhoeven, *Phys. Chem. Chem. Phys.* **2002**, *4*, 1542–1548.
[54] M. Latva, H. Takalo, V. M. Mukkala, C. Matachescu, J.-C. Rodriguez-Ubis, J. Kankare, *J. Lumin.* **1997**, *75*, 149–169.
[55] R. D. Archer, H. Y. Chen, L. C. Thompson, *Inorg. Chem.* **1998**, *37*, 2089–2095.
[56] P. Atkinson, K. S. Findlay, F. Kielar, R. Pal, D. Parker, R. A. Poole, H. Puschmann, S. L. Richardson, P. A. Stenson, A. L. Thompson, J. H. Yu, *Org. Biomol. Chem.* **2006**, *4*, 1707–1722.
[57] A. B. Pangborn, M. A. Giardello, R. H. Grubbs, R. K. Rosen, F. J. Timmers, *Organometallics* **1996**, *15*, 1518–1520.
[58] J.-C. G. Bünzli, C. Mabillard, *Inorg. Chem.* **1986**, *25*, 2750–2754.
[59] G. Schwarzenbach, *Complexometric Titrations*, Chapman & Hall, London, **1957**.
[60] E. R. Malinowski, D. G. Howery, *Factor Analysis in Chemistry*, Wiley, New York, Chichester, Brisbane, Toronto, **1991**.
[61] H. Gampp, M. Maeder, C. J. Meyer, A. D. Zuberbühler, *Talanta* **1986**, *33*, 943–951.
[62] R. Rodriguez-Cortinas, F. Avecilla, C. Platas-Iglesias, D. Imbert, J.-C. G. Bünzli, A. de Blas, T. Rodriguez-Blas, *Inorg. Chem.* **2002**, *41*, 5336–5349.
[63] J. C. de Mello, H. F. Wittmann, R. H. Friend, *Adv. Mater.* **1997**, *9*, 230–232.
[64] F. Gumy, **2007**, Patent application, PCT/IB2007/054187.
[65] C. Piguet, G. Bernardinelli, B. Bocquet, A. Quattropani, A. F. Williams, *J. Am. Chem. Soc.* **1992**, *114*, 7440–7451.
[66] J. F. Ajao, C. W. Bird, *J. Heterocycl. Chem.* **1985**, *22*, 329–331.
[67] C. E. Gutteridge, M. M. Hoffman, A. K. Bhattacharjee, L. Gerena, *J. Heterocycl. Chem.* **2007**, *44*, 633–637.
[68] H. Shinkai, T. Ito, H. Yamada, **2002**, US patent 6410561.
[69] I. A. Titova, T. I. Vakul'skaya, L. I. Larina, M. I. Mizandrontsev, V. A. Volkov, G. V. Dolgushin, V. A. Lopyrev, *Russ. J. Org. Chem.* **2005**, *41*, 1306–1315.
[70] M. Wozniak, M. Grzegozek, *Liebigs Ann. Chem.* **1993**, 823–829.
[71] U. Ries, P. Sieger, **2007**, USA, US patent 2007024595.

Received: September 10, 2008
Published online: December 9, 2008

